LRP 577/97 June 1997

Contributed Papers
presented at the
24th EPS CONFERENCE ON CONTROLLED
FUSION AND PLASMA PHYSICS

Berchtesgaden, Germany
9 - 13 June 1997

LIST OF CONTENTS

Effect of plasma shape on confinement and MHD behaviour in TCV

H. Weisen, S. Alberti, S. Barry, R.Behn, P. Blanchard, P. Bosshard, F. Bühlmann, R. Chavan, S. Coda, C. Deschenaux, M.J. Dutch, B.P. Duval, D. Fasel, A. Favre, S. Franke, I. Furno, T Goodman, M. Henderson, F. Hofmann, J-Ph. Hogge, P.-F. Isoz, B. Joye, J.B. Lister, X. Llobet, J.-C. Magnin, P. Mandrin, B. Marletaz, P. Marmillod, Y. Martin, J.-M. Mayor, J.-M. Moret, Ch. Nieswand, P. Paris, A. Perez, Z.A. Pietrzyk, V. Piffl[1], R.A. Pitts, A. Pochelon, K. Razumova[3], H. Reimerdes, A. Refke, J. Rommers, I. Roy[3], O. Sauter, W. Suttrop[2], W. van Toledo, G. Tonetti, M.Q. Tran, F. Troyon, P. Vyas and D.J. Ward

Centre de Recherches en Physique des Plasmas

École Polytechnique Fédérale de Lausanne

Association EURATOM-Confédération Suisse

CH-1015 Lausanne, Switzerland

[1]Institute for Plasma Physics, Czech Academy of Sciences, Prague

[2]Max-Planck Institut für Plasmaphysik, Garching, Germany, [3]RCC Kurchatov, Moscow

The TCV tokamak (B_T < 1.5T, R≈0.88m, a<0.25m) has produced a wide variety of plasma configurations, both diverted and limited, with elongations κ_a ranging from 0.9 to 2.58, triangularities δ_a from -0.7 to 1 as well as discharges with nearly rectangular cross sections. Plasma currents of 1 MA have been obtained in elongated discharges (κ_a≈2.3). Ohmic discharges with δ_a<0 have smaller sawteeth and higher levels of MHD mode activity than plasmas with δ_a>0. The main change in MHD behaviour when elongation is increased beyond 2 is an increase in the relative importance of modes with m,n>1 and a reduction of sawtooth amplitudes. Confinement is strongly dependent on plasma shape. In ohmic limiter L-modes energy confinement times improve typically by a factor of 2 as the plasma triangularity is reduced from 0.5 to 0 at constant q_a. There also is an improvement of confinement as the elongation is increased. In most discharges the changes in confinement are explained by a combination of geometrical effects and power degradation. A global factor of merit H_s (shape enhancement factor) has been introduced to quantify the effect of flux surface geometry. The introduction of H_s into well known confinement scaling expressions such Neo-Alcator and Rebut-Lallia-Watkins scaling leads to improved descriptions of the effect of shape for a given confinement mode. In some cases with $\kappa_a \geq 1.7$ limited ohmic L-modes undergo a slow transition to a confinement regime with an energy confinement improved by a factor of up to 1.5 and higher particle confinement. First experiments to study the effect of shape in ECRH at a frequency of 83 GHz (second harmonic) have been undertaken with 500 kW of additional power.

1.0 Introduction

Recent progress on the TCV tokamak has been marked by the attainment of highly elongated plasma cross-sections vertically stabilized by internal feedback coils with a bandwidth of 10 kHz [Hofmann et al, 1997], the implementation of two gyrotrons of 500 kW each for ECRH heating at the second harmonic of the cyclotron resonsance [Pochelon et al, 1997] and a campaign of systematic investigation of the effect of plasma shape on confinement and MHD behaviour. The design plasma current of 1MA has been attained in a discharge with an elongation at the LCFS κ_a=2.3 (fig. 1a) and B_T=1.43T. The highest elongation (κ_a=2.58) was obtained at I_p=725kA and B_T=1T (fig. 1b). The investigation of the effects of shaping have lead to the creation of unusual plasma shapes such as negatively triangular (fig. 1c), rectangular (fig. 1d) and rhomboidal (fig. 1e) cross sections [Moret et al 1997]. In addition a variety of diverted plasmas has been created for H-mode studies [Martin et al, 1997]. The plasma shape in these experiments was controlled using the MGAMS algorithm [Hofmann et al 1994].

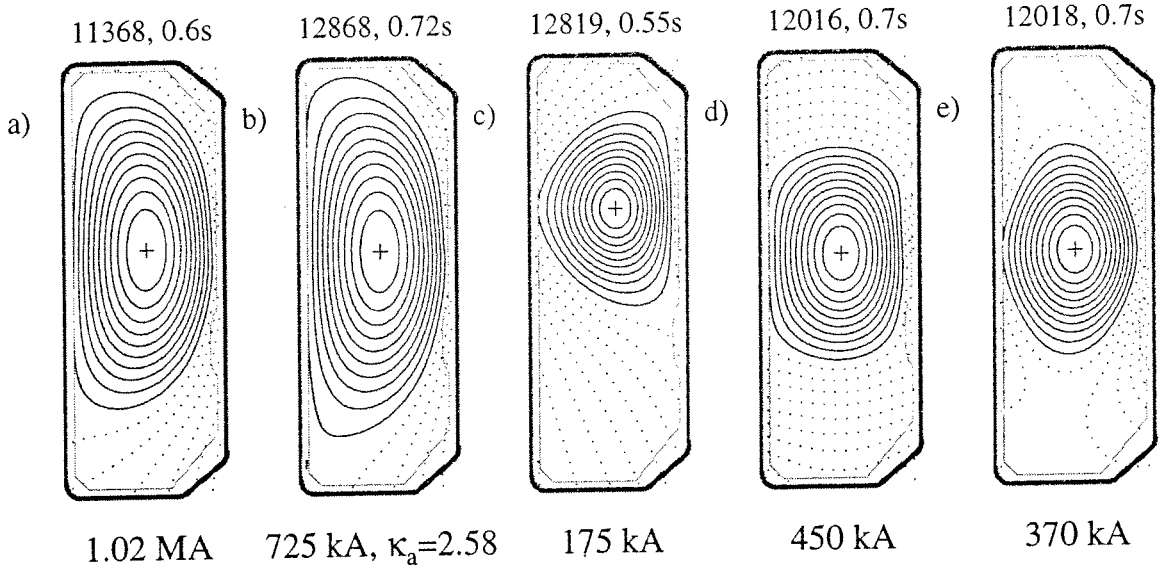

Fig. 1 Selection of plasma configurations recently produced in TCV.

2.0 Confinement in ohmic plasmas

The effect of shape on confinement was systematically investigated in a series of limited ohmic L-mode plasmas in which elongation κ_a, triangularity δ_a, edge safety factor q_a at the last closed flux surface and line average density $\bar{n}_e$ were systematically scanned in the range $1.06 < \kappa_a < 1.86, -0.41 < \delta_a < 0.72, 2.3 < q_a < 6, 2.85\times10^{19}m^{-3} < \bar{n}_e < 8.5\times10^{19}m^{-3}$, providing a database with 230 discharge conditions. The database has been extended with a selection of highly elongated limiter plasmas ($2 < \kappa_a < 2.5$) and diverted plasmas of moderate elongation in L-mode and in H-mode. Fig. 2a shows the electron confinement time, $\tau_{Ee} = W_e/P_{oh}$, where P_{oh} is the ohmic input power versus plasma edge triangularity δ_a in limited ohmic L-mode

plasmas for $\bar{n}_e \approx 6.3.10^{19}m^{-3}$ and $3 < q_a < 4$. The confinement increases as δ_a is reduced to zero and levels off or decreases slightly as δ_a is reduced below 0. Confinement time increases slightly with elongation. It should be noted that the ohmic power ranges from 200 kW for the smallest plasmas to 1.3 MW for the largest for the conditions shown in figure 2. The dependence seen in fig 2 is observed for the whole range of q_a and $\bar{n}_e$ investigated, although it is less pronounced at low q_a and low $\bar{n}_e$ [Moret et al 1996, Weisen et al 1997].

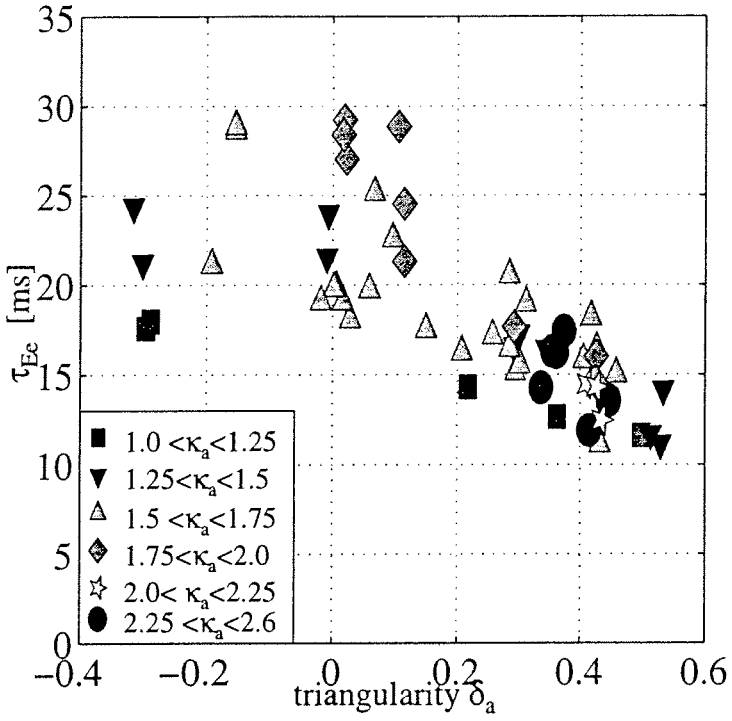

Fig. 2 Electron energy confinement time versus δ_a for $\bar{n}_e \approx 6.3.10^{19}m^{-3}$ and $3 < q_a < 4$.

The triangularity dependence may be the most surprising. We have ruled out variations in radiation losses as a cause for the dependence. Also the observed reduction of sawtooth amplitudes at low or negative triangularity cannot account for a factor-of-two effect [Weisen et al 1997]. In fig. 3 we show $\chi_{eff} = q_{oh}/(n_e\langle\nabla T_e\rangle)$ versus q_{oh} in the confinement zone ($r/a \approx 0.8$), where q_{oh} is the ohmic heat flux, n_e and $\langle\nabla T_e\rangle$ the local density and the flux surface averaged temperature gradient. The data are windowed in a narrow range of local densities and are shown for the whole range of δ_a investigated and $\kappa_a<1.9$. Despite the large triangularity dependence of τ_{Ee}, there is no significant dependence of $\chi_{eff} = \chi_e + \chi_i((n_i\nabla T_i)/(n_e\nabla T_e)) = q_{oh}/(n_e\langle\nabla T_e\rangle)$ on δ_a. Similarly little systematic dependence of χ_{eff} on κ_a can be discerned except in some cases of elongated plasmas at high density. The observation that χ_{eff} increases with q_{oh} offset-linearly, as indicated by the fitted line, shows that power degradation is already important in ohmic plasmas.

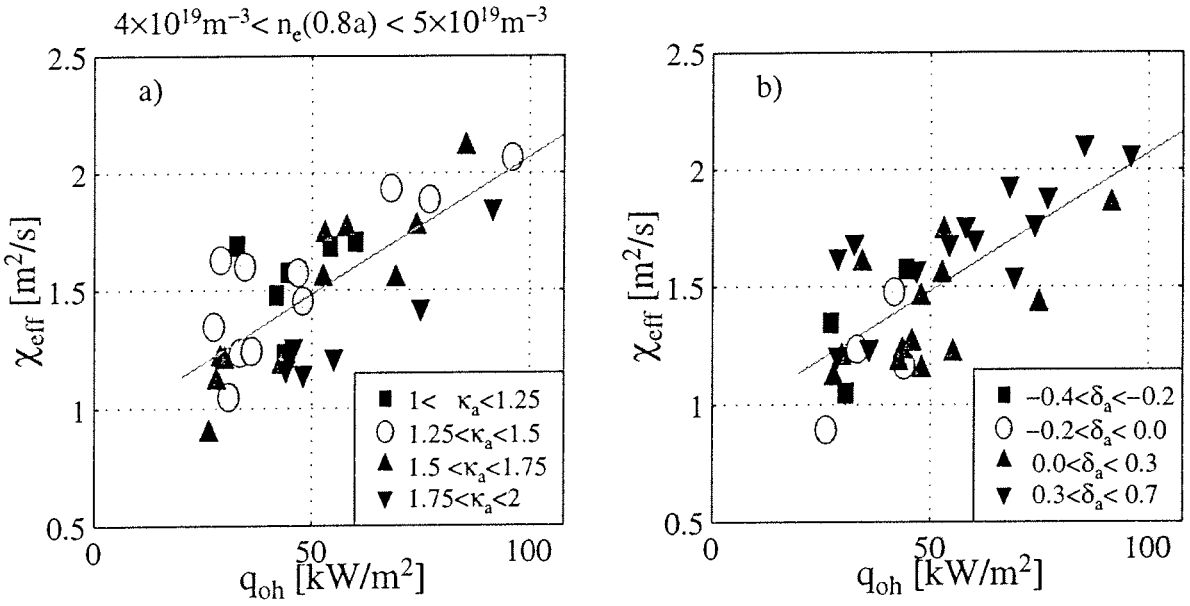

Fig. 3 Dependence of effective heat diffusivity in the confinement zone on ohmic heat flux for different classes of elongation (a) and triangularity (b) for $n_e \approx 4.5 \times 10^{19} m^{-3}$.

3.0 Geometrical effect of plasma shaping

A direct geometrical effect of the shaping is a modification of the flux surface separation and consequently of the temperature gradients. Since the existence of a relationship between fluxes and gradients is an established experimental fact [see e.g. Connor 1995 and references therein], shaping will influence the conducted heat flux for a given temperature profile. We define an effective minor radius coordinate r, chosen as the distance from the magnetic axis measured at the outer midplane and normalised such that $r = a$ on the last closed flux surface (LCFS). The heat flux may then be written as

$$q = -n\chi(dT/dr)(dr/d\psi)\nabla\Psi$$

The spatial distribution of the gradient geometrical factor, $(dr/d\psi)\nabla\Psi$, must be included in any analysis of the local energy balance. In the case of plasmas with negative triangularity or high elongation extended zones with favourable, high flux expansion arise near the tips while in the case of strong positive triangularity field lines are unfavourably compressed over a wide region at the low field side [Moret et al 1996].

4.0 Global shape enhancement factor

To quantify the influence of geometry alone, the energy confinement time of a shaped plasma can be compared with that of a cylindrical plasma having the same horizontal width, thermal diffusivity and heat flux, q, associated with the input power deposition profile. Assuming that the thermal diffusion coefficient depends neither on the poloidal angle nor on the temperature gradient, the temperature profile and the corresponding stored energy can be calculated by integration. We define a Shape Enhancement Factor H_s as the ratio of the confinement time to that of the reference plasma with the same profiles of $q/n\chi$ and of same density:

$$H_s = \frac{S_o \int_0^a \left(\int_r^a \frac{q}{n\chi} \frac{1}{\langle \nabla\Psi \rangle} \frac{d\Psi}{dr} dr' \right) n dV}{S \int_0^a \left(\int_r^a \frac{q}{n\chi} dr' \right) n dV_o} , \qquad [1]$$

where S symbolises the area of the LFCS and n can stand either for the electron or the ion density depending on context. Since the definition assumes the same heat flux for the reference and test case, the ratio of stored energies in the above expression has been multiplied by the ratio of total powers which is equal to S_o/S. The normalization with S_o/S also removes any trivial scaling of H_s with plasma volume. Values of $H_s > 1$ imply an improvement of energy confinement with respect to a circular plasma. The inner integral in expression 1 is a weighted average of $(dr/d\psi)\langle\nabla\Psi\rangle$ by the profile of $q/(n\chi)$. This is chosen to be equal to $-dT_o/dr$ where T_o is the normalized temperature profile of the reference plasma. Hence it is not necessary to know the profiles of heat diffusivity, heat deposition and density a priori if an experimental reference discharge is available. The temperature profiles in the experiments described are approximately trapezoidal, which is characteristic of sawtoothing ohmic discharges. Fig. 4 shows how H_s depends on δ_a and κ_a for the discharges investigated. We chose T_o to be the average of the normalised temperature profiles of the plasmas studied. We also assumed a flat density profile for simplicity. Note that H_s scales linearly with κ_a.

4.1 Confinement scaling using the global shape enhancement factor

Since H_s in eq. 1 is defined under the assumption of a given heat flux, the effect of variations of the heat flux must be included in order to account for power degradation. In fig.5 we show the confinement times of the same data that are shown in fig 1, corrected for shape and power degradation by multiplying them using a factor proportional to $H_s \times (P_{oh}/S)^{-0.5}$. The measured profiles were used for each data point in the evaluation of H_s.

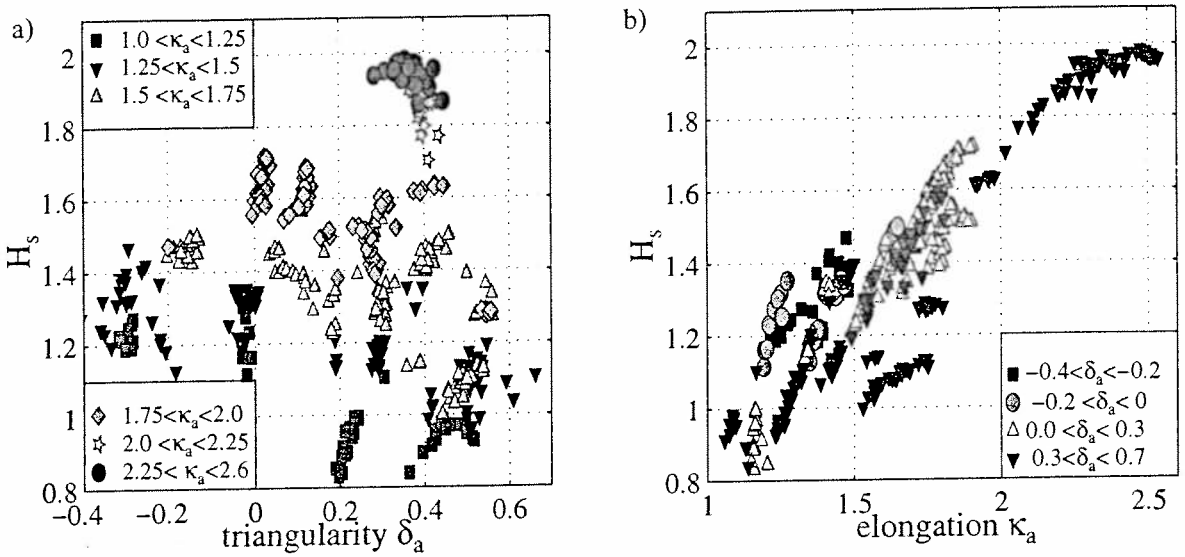

Fig. 4 Dependence of global shape enhancement factor on a) triangularity and b) elongation.

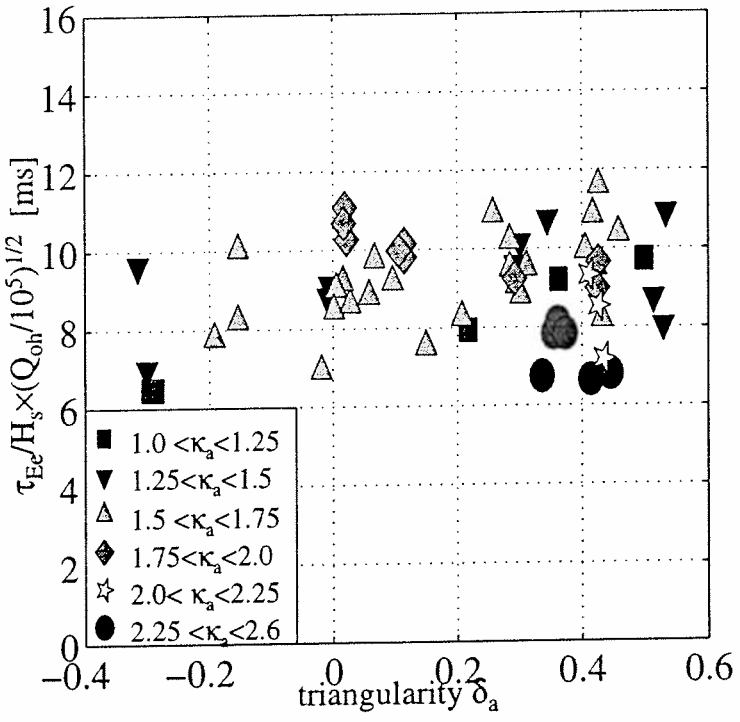

Fig. 5 Electron energy confinement times corrected for shape and power degradation.

H_s can be used in global scaling expressions to describe the effect of geometry [Weisen et al 1997]. Prior to exemplifying this with Neo-Alcator scaling [Uckan 1990] we have to consider the response of ohmic plasmas to confinement changes. Assuming Spitzer conductivity

($\sigma = c_\sigma T_e^{3/2}$) it can be shown that a change in confinement time will result in a modest change in plasma temperature

$$T_e(0) = \left\{ \frac{2j^2(0)}{3ec_\sigma} \cdot \frac{2\pi AR}{V} \cdot \frac{\langle p_e^* \rangle}{\langle \sigma^* \rangle} \cdot \frac{\tau_{Ee}}{n_e(0)} \right\}^{2/5} \qquad [2]$$

and a more pronounced change in ohmic power

$$P_{oh} = \left[\frac{27e^3}{8c_\sigma^2}\right]^{1/5} \cdot \left[\frac{2\pi R}{A}\right]^{2/5} \cdot V^{3/5} \cdot \frac{\langle p_e^* \rangle^{3/5}}{\langle \sigma^* \rangle^{2/5}} \cdot I_p^{4/5} \cdot \left[\frac{n_e(0)}{\tau_{Ee}}\right]^{3/5} \qquad [3]$$

where $<p_e^*> = <p_e/p_e(0)>_V$ is the volume averaged electron pressure normalized to the central pressure and similarly $<\sigma^*>$ is a profile width factor for the Spitzer conductivity profile, A is the cross sectional area, V the volume and I_p the toroidal current of the plasma [Weisen et al 1997]. The above equations are well adhered to in TCV as seen in fig.6a where the measured loop voltage is plotted versus the loop voltage derived from eq.3. The ratio of profile width factors is close to unity throughout our entire database including L and H-modes of all shapes, including central elongations up to 2.1, with $\langle \sigma^* \rangle \cong 0.4 \langle j \rangle^*$, where $<j>^* = \mu_0 R_0 <j>/B_T$ is a non-dimensional average current density (fig.6b). These relationships appear to be at least qualitatively consistent with theoretical considerations based on minimum energy states [Biskamp 1986, Kadomtsev 1987] or stationary entropy [Minardi 1997].

The confinement time depends itself on heat flux through the effect of power degradation, which can be expressed by an empirical relation of the form $\tau_{Ee} = \tau_{eE0}(Q/Q_0)^{-\alpha}$ [4] where Q is the heat flux through the last closed flux surface, Q_0 refers to a reference case, and τ_{Ee0} is an underlying confinement time. The effect of power degradation amplifies any underlying changes of confinement in ohmic plasmas, as seen when combining eq.4 with the lead dependencies in eqs. 2 and 3: $\tau_{Ee} = \tau_{Ee0}^{\gamma}$ where $\gamma = 1/(1-3\alpha/5)$ [5]. For α=0.5, which is typical for most tokamak experiments including ohmic TCV discharges, γ is equal to 10/7.

In fig 7a we show the total confinement time from kinetic measurements (restricted to $Z_{eff}<3$ and $P_{rad}/P_{oh}<0.4$) versus the Neo-Alcator (NA) scaling expression [Uckan 1990]. NA scaling contains neither shape dependence nor power dependence terms. Although agreement is good for plasmas at low elongation, NA scaling fails to predict confinement in highly elongated plasmas by a factor of three (upper broken line). An immediate improvement is obtained when multiplying the NA scaling by the factor $H_s^{10/7}$ thereby taking into account shape and power degradation simultaneously. A further improvement is obtained by replacing the edge safety factor in the original expression by $<j>^*$ and by fitting the density dependence to obtain (fig 7b):

$$\tau_{NA\text{-}TCV} = 0.17 \times a R_0^2 H_s^{10/7} \langle 10^{-20} n_e \rangle^{0.78} / \langle j \rangle^* \qquad [6]$$

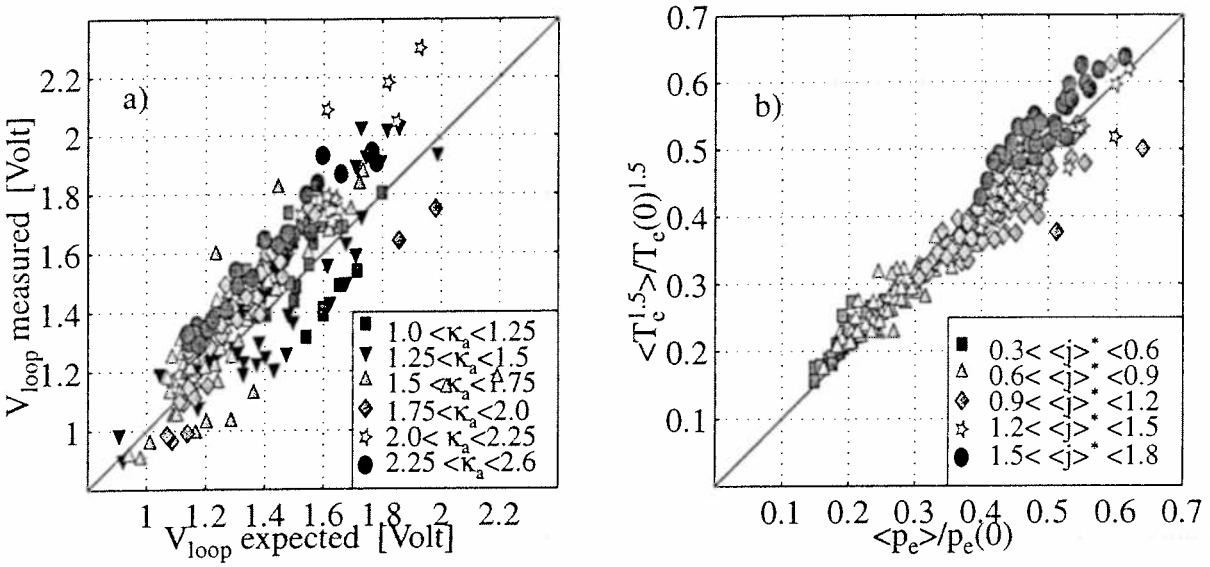

Fig. 6 a) V_{loop}, measured versus expected from eq.3. b) Relationship between profile width factors for Spitzer conductivity and electron pressure.

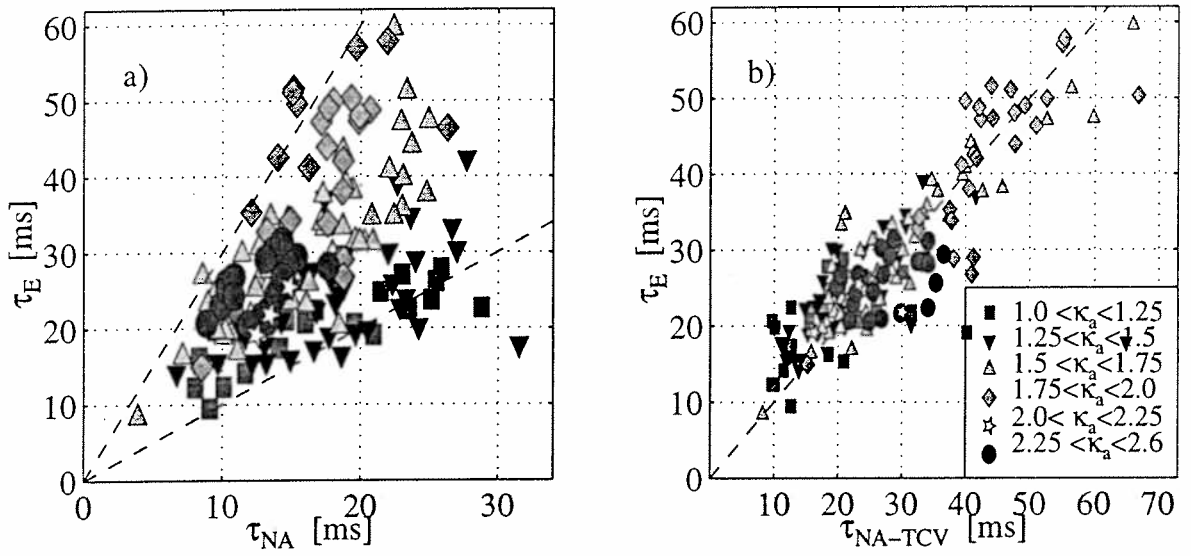

Fig. 7 Total confinement time in TCV versus a) Neo-Alcator scaling b) NA-TCV scaling. The data shown also include 'square' and diverted L-modes.

Good agreement is found with RLW scaling [Rebut et al 1987] due to its strong scaling with elongation, the introduction of H_s in RLW scaling essentially correcting for the effect of triangularity [Weisen et al 1997] or squareness [Moret et al 1997].

Many discharges at elongations higher than about 1.7 are characterized by a phase with a spontaneous density and temperature rise, which indicates that they overcome the usually observed

'soft' saturation of confinement where the temperature drops slowly as density is increased [Nieswand et al 1997]. The improvement can be anywhere in the range between 1 and 1.5, which is too small to be visible as differentiated set of data in fig.7. These discharges may be related to the IOC mode observed on ASDEX [Bessenrodt Weberpals et al, 1991].

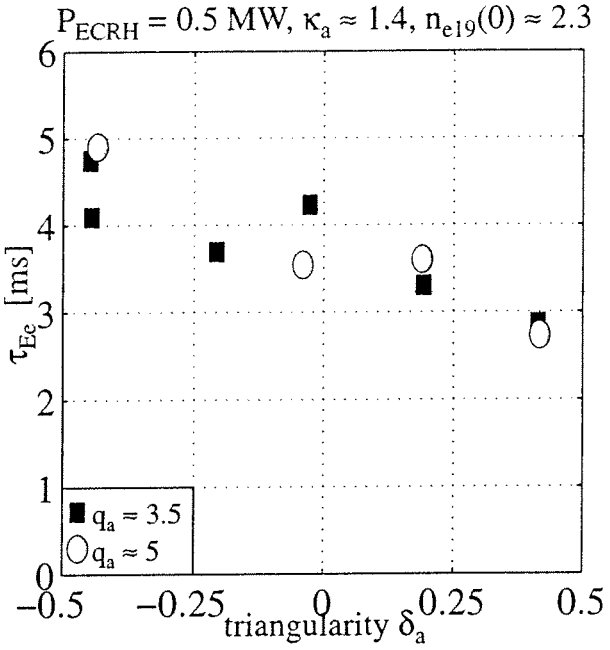

Fig.8 shows electron energy confinement times of ECR-heated plasmas at $n_e(0) \approx 2.3 \times 10^{19} m^{-3}$ with P_{ECRH}=0.5 MW for q_a=3.5 and q_a=5 in a triangularity scan. The confinement time exhibits similar trends as observed in ohmic plasmas. The interpretation of ECRH confinement experiments is complicated by the sensitivity of the plasma response to the power deposition profile, which, if peaked near the q=1 surface alters the sawtooth behaviour. (Pochelon et al. 1997).

Fig. 8 Confinement times of ECR heated plasmas (0.5 MW) versus triangularity.

5.0 MHD behaviour

The amplitude of sawtooth crashes varies strongly with triangularity, being largest at positive triangularity and sometimes vanishing at negative triangularity, as seen at the top of figure 9. The amplitude of non-axisymetric MHD modes, presumably tearing modes, shows the opposite behaviour with δ. These consist of brief bursts at or near the sawtooth crash for $\delta>0$ but can become continuous for $\delta<0$ and lead to loss of confinement, locked modes and cause disruptions. The reduction of sawtooth amplitudes is only partly explained by a slight reduction in inversion radius at $\delta<0$ (bottom of fig.9), due to a reduction of average current density when δ is reduced at constant q_a, and a slight reduction in sawtooth period by typically a factor of 1.5. Fig.10a shows the central post-crash reheat power density versus core ohmic heating power density as estimated from tomography. The difference between the reheat power and the heating power is attributed to equipartition. The figure shows that post-crash reheating is strongly dependent on input power. Any reduction of ohmic power, as may result from

improvements in confinement will reduce the reheat power and affect sawtooth amplitudes. Note the inverse correlation in fig. 10a of confinement times and reheat power.

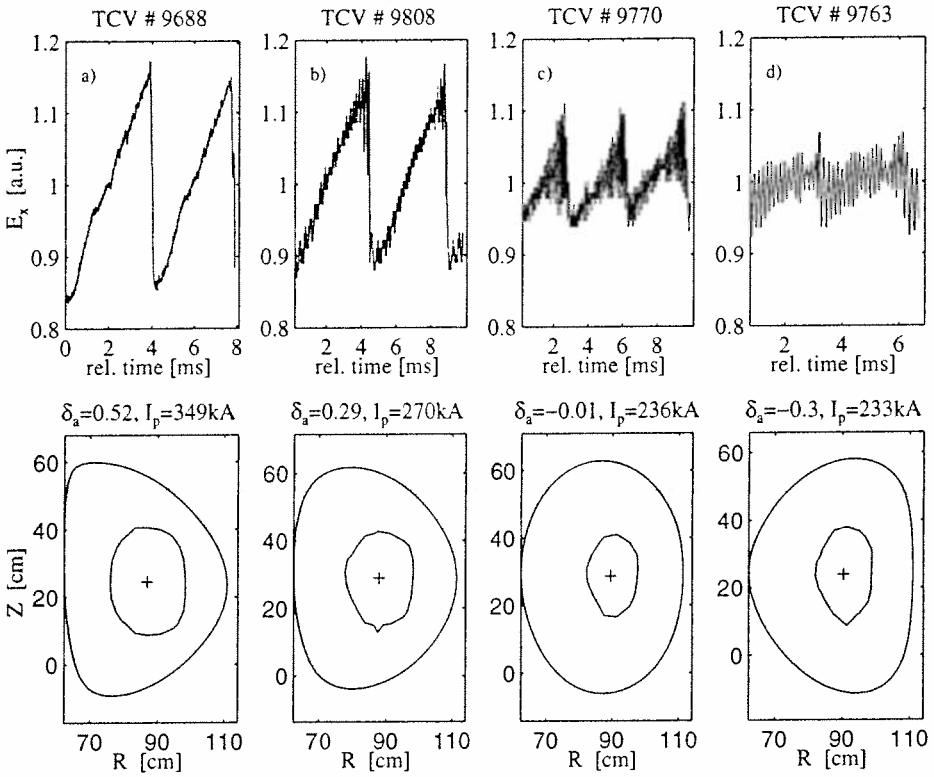

Fig. 9 Sawtooth inversion radius from X-ray tomography (bottom,inner contours) and LCFS (outer contours) for four different triangularities. Raw X-ray signal with sawtooth and Mirnov oscillations (top) for q_a=3.5, $\bar{n}_e = 5.0 \cdot 10^{19} m^{-3}$, κ_a=1.4.

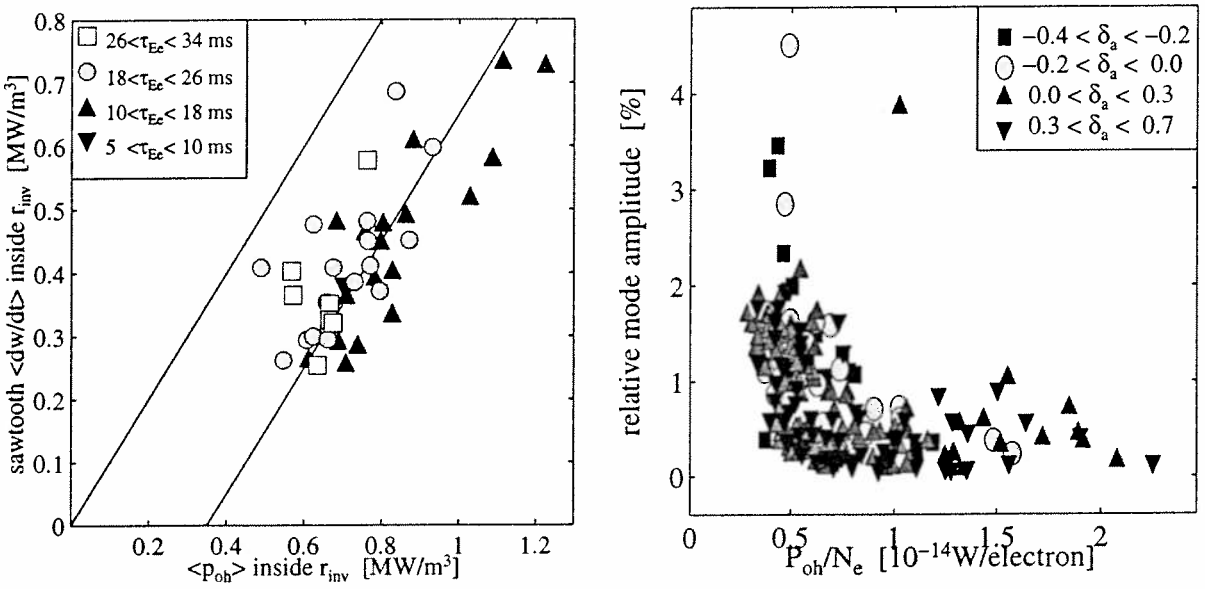

Fig. 10 a) Sawtooth reheat power density versus central ohmic power for $n_e = 6.3 \cdot 10^{19} m^{-3}$. b) Relative amplitude of MHD modes from x-rays versus power/electron for κ_a<1.9.

The increase of mode activity at reduced triangularity may, at least in part, also be attributed to a reduction in ohmic heating power. This is shown in figure 10b where the relative mode oscillation amplitude from a line integrated X-ray measurement, is plotted versus loss power per electron, P_{oh}/N_e. This quantity is itself strongly correlated with the electron temperature in the boundary region, measured at r/a=0.9 increases with P_{oh}/N_e from near 100 eV to near 350 eV over the range of the abscissa in figure 10b. The symbols refer to classes of triangularity. In the majority of cases mode amplitude correlates well with P_{oh}/N_e and boundary temperature. High amplitude modes are unlikely to develop with Te(0.9a) > 200 eV, but are quite frequent at lower temperatures. Since most of the occurences of very high mode amplitudes in fig10b occur with $\delta<0$ an intrinsic dependence of mode stability on δ cannot be excluded. If proneness to resistive modes is solely a matter of heat flux to the edge or of edge temperature there is scope to suppress these modes by additional heating. Recent ECRH experiments with $\delta<0$, have not yet been able to test this idea because at the very low densities of these experiments ($n_e \sim 2\times10^{19} m^{-3}$) discharges with $\delta<0$ obtained so far do not appear to develop such mode activity even with ohmic heating alone.

The modes observed using x-ray tomography consist of a superposition of m=1,2 and sometimes m=3 modes, with amplitudes peaking at the sawtooth inversion radius [Furno et al 1997]. A set of 4 toroidally equally spaced vertically viewing diodes allows us to distinguish between n=1 or 3 and n=2 modes. As κ_a is increased beyond 2, the relative importance of n=2,m=2 modes increases and sawtooth amplitudes decrease. Operation at elongations beyond 2.2 is currently limited by MHD modes appearing at low q_a and vertical stability at high q_a [Hofmann et al. 1997]. These difficulties may be overcome in the future by the development of discharge scenarios involving different plasma shapes, lower density or ECRH heating.

6.0 Conclusions

Large variations of confinement time have been observed in shaping experiments in ohmic L-mode plasmas in TCV. Variations in MHD behaviour such as amplitudes of sawtooth crashes and of presumably resistive MHD modes appear in most cases as a consequence of the large changes in ohmic heating power in these experiments, which in turn depends on confinement. We have ruled out radiation losses and prompt energy losses due to sawteeth as explanations for the dependence of confinement on shape. However we should emphasize that the results were obtained at $\beta_N<2$. The improvement of confinement time as triangularity is reduced may only

apply to discharges at low β since the geometrical shear introduced by triangularity has a stabilizing effect on ballooning modes and ELMs [Hyatt et al. 1994, Itami et al. 1995, JET Team 1995]. The large variation in the measured energy confinement time within the domain of explored equilibria can be explained by direct geometrical effects of shaping combined with heat flux degradation. The effect is successfully described by a shape enhancement factor H_s which is based on a ratio of stored energies of a shaped plasma to that of a cylindrical reference plasma with the same heat flux. Where confinement time changes with shape are not described by H_s, these can be interpreted as being due to changes in the transport coefficients. The introduction of H_s in the international confinement database has the potential of improving the description of the effect of shape for a given confinement mode and the prediction for future devices. It remains however to be verified if H_s is as successful for plasmas with auxiliary heating and for different confinement regimes as it is for these ohmic L-mode discharges.

Acknowledgement: This work was partly supported by the Swiss National Science Funds.

References:

Bessenrodt-Weberpals M. et al, *Nuclear Fusion* **31**, 155 (1991)

Biskamp D., *Comments Plasma Phys. Control. Fusion* **10**, (1986) 165

Connor J.W., *Plasma Phys. Control. Fusion* **37**, A119 (1995)

Furno I. et al, contributed papers, this conference (1997)

Hofmann F. et al, *Plasma Physics Contr. Fusion* **36**, B277 (1994)

Hofmann F. et al, contributed papers (and references therein), *this conference* (1997)

Hyatt A.W. et al, *21st EPS Conf. on Contr. Fusion and Plasma Phys*, ECA **18B**, p. I-14 (1994)

Kadomtsev B, *Proc. International Conference on Plasma Physics*, Kiev, 6-12.4 (1987), 1273, edited by A.G. Sitenko, published by World Scientific

Itami K. and the JT-60 Team, *Plasma Phys. Contr. Fusion* **37** (1995) A255

JET Team (presented by T.T.C. Jones), *Plasma Phys. Contr. Fusion* **37** (1995) A359

Martin Y. et al, contributed papers, *this conference* (1997)

Minardi E. report FP 97/3, Istituto di Fisica del Plasma, Via Bassini 15, I-20133 Milano (1997)

Moret J.M., *subm. to Phys. Rev. Lett (1996), also CRPP report* LRP 560/96.

Moret J.M. et al, contributed papers, *this conference* (1997)

Nieswand Ch. et al, contributed papers, *this conference* (1997)

Pochelon A. et al, contributed papers, *this conference* (1997)

Rebut P. H., Lallia P. P. and Watkins M.L. *JET report* **JET_P(88) 05** and corrigendum.

Uckan N.A. and ITER Physics Group, *ITER Physics Design Guidelines: 1989, ITER documentation series, No 10, IAEA, Vienna* 1990.

Weisen H. et al, (and refs. therein) to be published in *Nuclear Fusion*, available from the authors as *report* ***LRP* 571/97** (1997)

Stability and Energy Confinement of Highly Elongated Plasmas in TCV

F. Hofmann, R. Behn, M.J. Dutch, Y. Martin, J.-M. Moret, C. Nieswand, Z.A. Pietrzyk, H. Reimerdes, D.J. Ward

Centre de Recherches en Physique des Plasmas
Ecole Polytechnique Fédérale de Lausanne
Association EURATOM - Confédération Suisse
CH- 1015 Lausanne, Switzerland

1. Introduction

One of the principal aims of TCV [1] is the creation and active stabilization of highly elongated plasmas, $\kappa \leq 3$. This implies high growth rates of axisymmetric modes and a very low stability margin. To stabilize such modes, TCV is equipped with a vertical position control system using a combination of slow coils outside the vacuum vessel (response time $\approx$ 1ms) and a fast coil inside the vessel (response time $\approx$ 0.1ms). The fast coil became operational in August 1996 and this paper describes the first experiments using both fast and slow coils for vertical stabilization.

2. Axisymmetric Modes

The dominant axisymmetric mode in an elongated tokamak is basically a vertical displacement of the entire plasma. The open-loop growth rate of this instability depends primarily on plasma elongation but also on a number of other parameters, such as triangularity, squareness, vertical position within the vessel, plasma wall distance, internal inductance, poloidal beta, etc. [2,3].

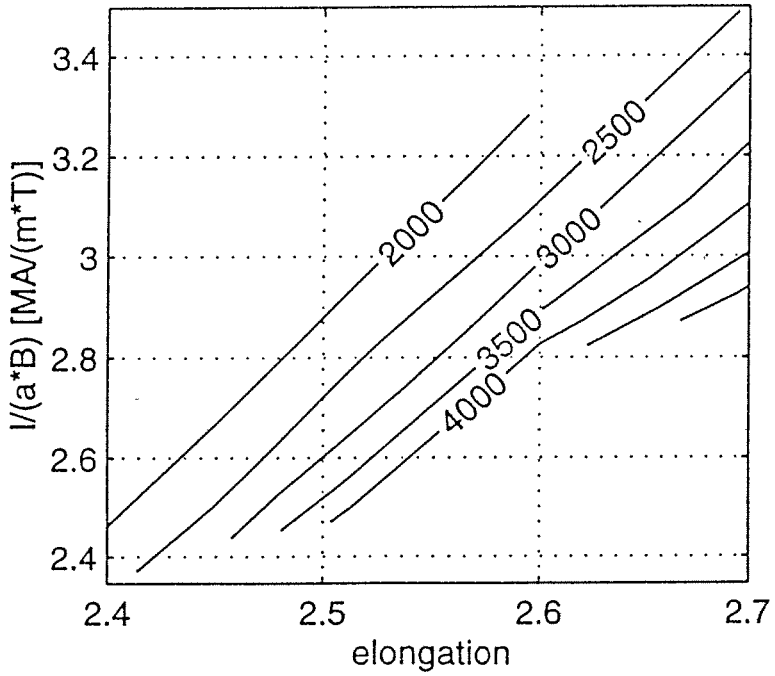

Fig.1.: n=0 growth rate [sec^{-1}] for D-shaped plasmas in TCV

If these other parameters are optimized to give the minimum growth rate for a given elongation, and if we assume Ohmic current profiles and low beta ($\beta_{tor} \approx 2\%$), we can express the vertical growth rate as a function of elongation and normalized current (Fig.1). The results presented here have been computed with the NOVA-W code [4]. Vertical instability growth rates have also been measured in TCV and excellent agreement with NOVA-W results was found [3].

3. Experiments with Slow Coils Only

The power supplies which drive the slow coils in TCV i.e. the shaping coils outside the vacuum vessel, have a response time, Δt, of approximately 1ms. This imposes an upper limit on the growth rate that can be stabilized with these coils, $\gamma < (\Delta t)^{-1}$ [5]. In fact, plasmas with vertical growth rates up to 1000 sec^{-1} have been successfully stabilized in TCV with the slow coils only [3]. An upper limit on the growth rate implies an upper limit on elongation for any given plasma current, as is evident from Fig.1.

4. Experiments with Slow and Fast Coils

The fast coil in TCV is mounted inside the vacuum vessel and consists of 6 turns connected in series, 3 positive turns on the bottom and 3 negative turns on the top of the vessel. The coil is driven by a power supply capable of producing a maximum current of 2kA at 550V with a response time of less than 0.1ms. Initial experimemts with the fast coil were done on plasmas with low current (250kA), low triangularity and large plasma-wall distance (Fig.2a). Under these conditions, the growth rate of the vertical instability is large, even at moderate elongation (κ=1.9). Derivative feedback was applied to the fast coil and four outboard slow coils, whereas proportional feedback was only applied to the slow coils. This scheme ensures that the time-averaged current in the fast coil always remains close to zero. Optimization of the three feedback gains (slow proportional gain, slow derivative gain and fast derivative gain) allowed us to stabilize plasmas with vertical growth rates up to 4400 sec^{-1}, corresponding to a stability margin, f=1.028.

After the system had been shown to work satisfactorily at low plasma current, a second series of experiments was launched with the aim of maximizing the plasma current. For this purpose, the triangularity was increased, the plasma was moved to the top of the vessel and the plasma current was increased to a value close to the q=2 limit. The feedback scheme was the same as the one used for the low current experiments. Using a toroidal field of 1.43 T, a maximum current of 1.02MA was reached at an elongation of κ=2.28 (Fig. 2b). This plasma had a relatively modest vertical growth rate, γ = 1200 sec^{-1}.

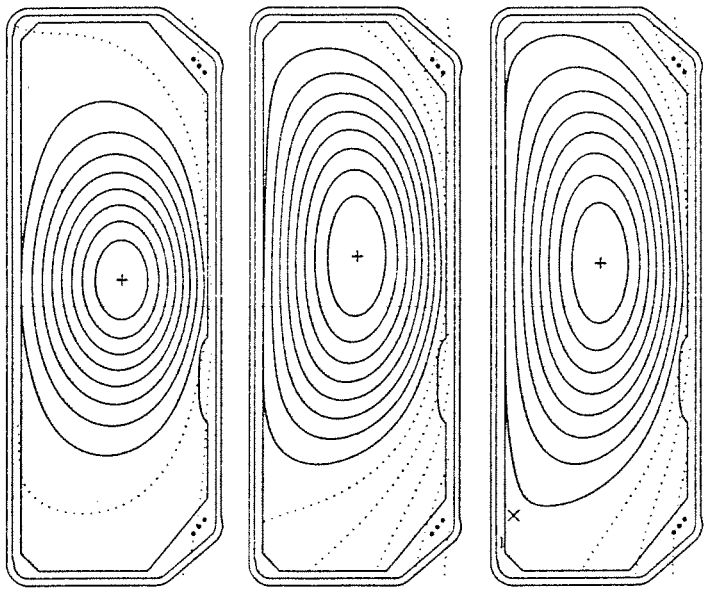

Fig.2.: Reconstructed equilibria of TCV discharges

(a)	*(b)*	*(c)*
I_p=*257kA*	I_p=*1.024MA*	I_p=*726kA*
B_t=*1.43T*	B_t=*1.43T*	B_t=*1.00T*
κ=*1.93*	κ=*2.28*	κ=*2.58*

A third series of experiments was then undertaken to explore the limits on elongation. This was done at a lower toroidal field, 1.0T, in order to minimize the risk of damage to the fast coil during vertical disruptions. The feedback setup was still the same as was used for the previous experiments, but the vertical position observer was slightly modified such as to minimize its sensitivity to the fast coil current. These experiments led to the successful stabilization of D-shaped plasmas with elongations up to 2.58 (Fig.2c) and vertical instability growth rates up to 2700 sec^{-1}.

5. Current Limit at High Elongation

During the experimental campaign described above, it was found that the maximum normalized current that can be stably confined increases with elongation, as expected, up to $\kappa \approx 2.3$. However, for $\kappa > 2.3$, the maximum normalized current remains roughly constant, $I_p/(a*B) \approx 3.0*10^6$ (Fig.3.). As soon as we try to increase the current above this limit, non-axisymmetric modes appear and lead to a disruption. The modes have been analyzed using toroidal and poloidal arrays of fast pick-up coils and mode numbers m/n=3/2 or m/n=2/1 are observed just before the disruption. This result is consistent with theoretical predictions [6,7] indicating that the current limit at zero pressure is approximately given by $I_p/(a*B) < 3.2*10^6$ at an elongation $\kappa=2.5$ and remains constant up to $\kappa=3.0$. Based on these results, we can now draw operational limits in κ-I_p space and we find that the maximum elongation that can be produced in TCV depends on the maximum vertical growth rate that can be stabilized.

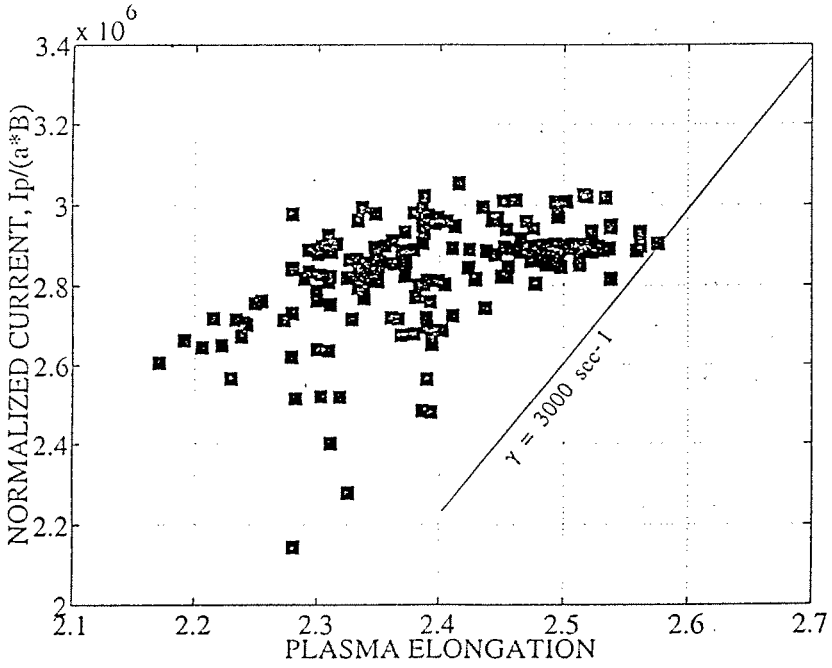

Fig.3.: Normalized current vs. elongation for TCV plasmas

Since the fast coil has a response time of less than 0.1ms, it is possible to stabilize very high growth rates, of the order of 5000 sec^{-1}. However, for a growth rate of this magnitude, the stability margin is extremely small, f=1.025, and a very slight change in plasma position or current profile (ELMs, sawteeth) can then push the plasma beyond the ideal limit (f=1). In order to avoid this extreme sensitivity, we assume, as a practical limit, $f \geq 1.042$, which implies $\gamma \leq 3000$ sec^{-1} in TCV. Together with the current limit mentioned above, this leads to an upper limit on elongation, $\kappa \leq 2.6$ (Fig.3.). This limit is, of course, only valid for conventional D-shaped plasmas and does not apply to more exotic shapes such as doublets [8] or triplets [9].

6. Confinement at High Elongation

The experiments with highly elongated plasmas have produced an additional, rather unexpected result. It was observed that, above a certain elongation, the plasma undergoes a slow transition, typically within 200ms, to a new mode of operation. This new mode is characterized by higher electron density, higher electron temperature, slightly lower loop voltage and a higher energy confinement time. A typical example is shown in Fig.4. The transition takes place during the current plateau, between 300 and 500ms. It is likely that the transition is associated with a change in current profile, as the internal inductance is increasing (Fig.4.).

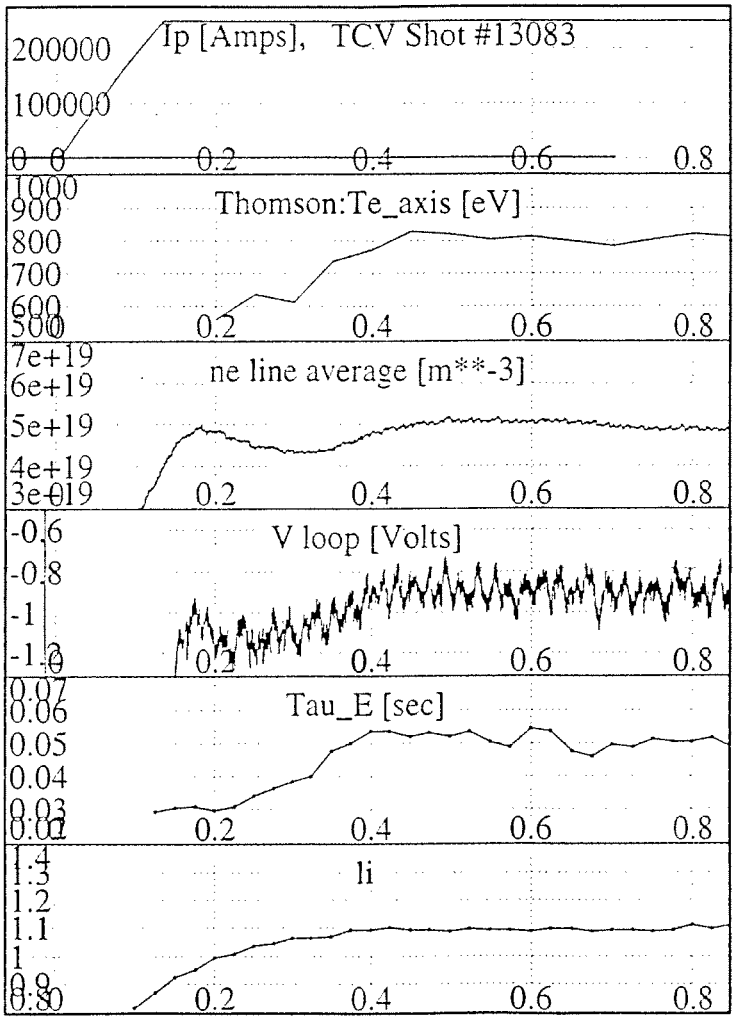

Fig.4.: Transition to a state of improved Ohmic confinement

Acknowledgements

It is a pleasure to acknowledge the competent support of the entire TCV team. This work was partly supported by the Fonds National Suisse de la Recherche Scientifique.

References

[1] Hofmann, F. et al., Plasma Phys. Control. Fusion **36** (1994) B277.

[2] Ward, D.J. et al., Nuclear Fusion **33** (1993) 821.

[3] Hofmann, F. et al., Nuclear Fusion **37** (1997) 681.

[4] Ward. D.J. et al., J. Comput. Phys. **104** (1993) 221.

[5] Noll, P. et al., in Controlled Fusion and Plasma Heating (Proc. 17th Europ. Conf. Ansterdam, 1990), Part I, Vol. 14B, 419.

[6] Turnbull, A.D. et al., Nuclear Fusion **29** (1989) 629.

[7] Eriksson, G. et al., in Plasma Physics (Proc. 1992 Int. Conf. Innsbruck), Vol. 16C, Part I, European Physical Society (1992) 343.

[8] Wesley, J.C. et al., in Plasma Phys. Contr. Nuclear Fusion Research 1980 (Proc. 8th Int. Conf. Brussels, 1980) Vol 1, IAEA (1981) 35.

[9] Hofmann, F., Plasma Physics and Controlled Fusion **29** (1987) 1053.

Observation of Improved Ohmic Confinement in Highly Elongated TCV Discharges

C.Nieswand, F.Hofmann, R.Behn, I.Furno, J.-M.Moret, Z.A.Pietrzyk, A.Pochelon, H.Reimerdes, H.Weisen

Centre de Recherches en Physique des Plasmas
Ecole Polytechnique Fédérale de Lausanne
Association EURATOM-Confédération Suisse
CH-1015 Lausanne, Switzerland

1 Introduction

The primary goals of the TCV tokamak are to produce plasmas with high elongation and to investigate confinement behaviour for a variety of plasma shapes [1]. A spontaneous transition to an improved ohmic confinement regime has recently been observed in moderately and highly elongated discharges limited by the central column. The observed features are similar to those observed in ASDEX (IOC regime).

2 General Observations during Improved Confinement

The transition to improved confinement is characterized by a spontaneous increase of plasma density, by about 10%, even when the external gas fuelling is reduced and a simultaneous increase of the electron temperature by more than 15%. Thus the total stored energy grows and the loop voltage and consequently the ohmic heating power drop. Both effects yield an improvement in β and the global energy confinement deduced from the equilibrium reconstruction code and confirmed by Thomson scattering measurements. The neutron rate and the Soft X-ray emissivity grow substantially and Z_{eff} is only moderately increased from 1.8 to 2.2.

Unlike ohmic ELM-free H-modes, where in general the density rises uncontrollable, this confinement mode can be maintained for the entire current flat top of more than one second. The plasma density saturates after the transition since the density feedback reduces the gas fuelling. Changes in the D_α emission can be attributed to this reduction of fuelling rather than to a change in particle transport or recycling near the edge. A slight change of the internal plasma inductance l_i, modifications of density and temperature profiles and changes of the sawtooth behaviour indicate that particle and energy transport are affected in the whole plasma volume.

2.1 Low Plasma Current

The transition was first observed in discharges at low current and moderate elongation (240-300kA, $q_{95} \approx 5$, κ=1.6-1.9, $\delta \approx 0.25$, $B_t = 1.43$T). In these plasmas the transition occurres

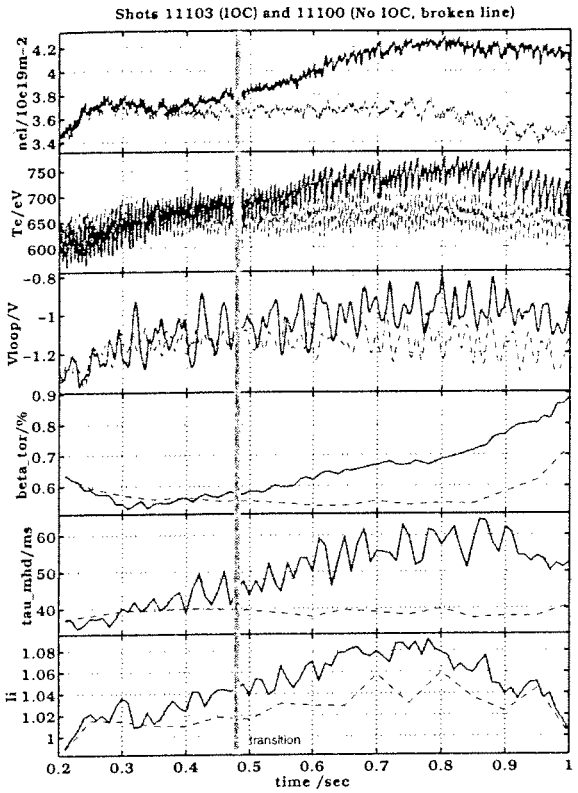

Figure 1: Comparison of an IOC plasma (solid lines) and a non IOC plasma (broken lines). (255kA, $q_{95} \approx 5$, κ=1.8, δ = 0.28, B_t = 1.43T)

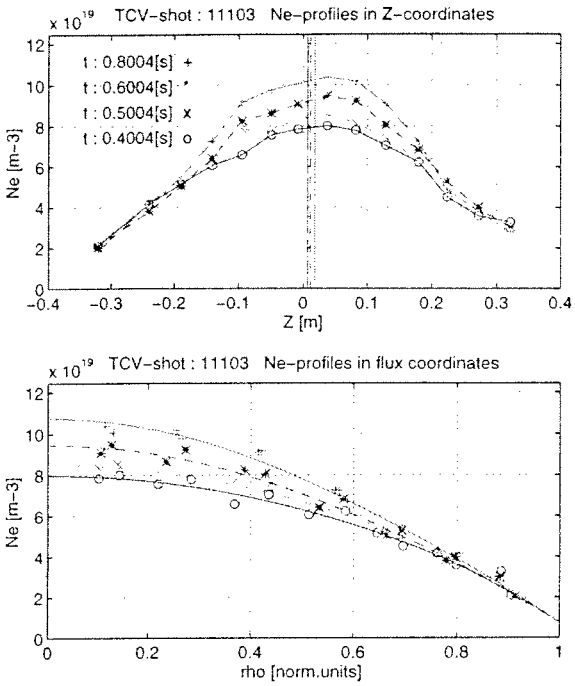

Figure 2: Electron density profile peaking during improved confinement at low current

during the current flat top when the plasma configuration is fully established (see figure 1). The electron energy confinement time deduced from Thomson scattering data increased from 16ms to 30ms after the transition. The equilibrium reconstruction reveals higher values. For "normal" confinement the energy confinement time saturates at high density, while plasmas with improved confinement do not show this behaviour.

The sawtooth period grows after the transition and in a few cases the sawtooth activity disappears completely. Soft X-ray tomography does not indicate a significant change in the q=1 surface position.

The electron density profile clearly peaks after the transition, caused by an increase of the central density whereas the edge density remains constant (figure 2). The central electron temperature increases slightly. This indicates a small change of the current density profile also suggested by an increase in the plasma inductance.

2.2 High Plasma Current

In highly elongated plasmas at high current (500-800kA, $q_{95} \approx$ 2-3, κ =2-2.5, $\delta \approx 0.25$) the transition occurs during the shaping phase of the scenario and sometimes even before the current flat top is reached (figure 3). Changes due to modifications of the configuration and due to a transition are therefore difficult to distinguish. An improvement of the electron energy confinement time from 12ms up to 20ms was observed. The highest value of β_{tor} of

2.9% ever achieved in TCV (as obtained from purely magnetic equilibrium reconstruction) was obtained under these conditions.

In contrast to the low current case the sawtooth period usually shortens and strong MHD activity often leads to minor or even major disruptions. Analysis of the signals of poloidal and toroidal magnetic probes suggest an (n=2,m=3) structure for the dominant mode, which grows during a few milliseconds and disappears shortly before the disruption (figure 4). Presently the operational domain of TCV at high elongation is limited on the low current side by the vertical instability and on the high current side by non-axisymmetric MHD activity [2].

The electron temperature profiles are essentially flat near the centre with indications of

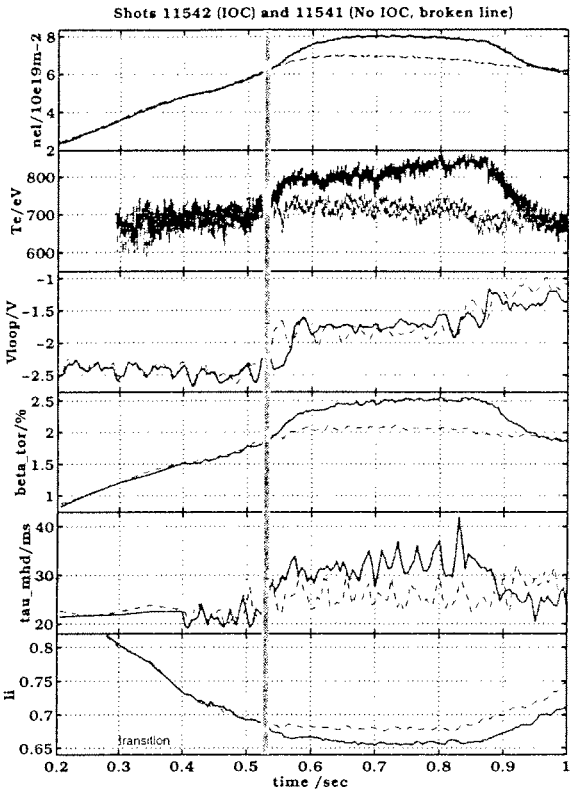

Figure 3: Comparison of an IOC plasma (solid lines) and a non IOC plasma (broken lines). (710kA, $q_{95} \approx 3$, κ=2.3, $\delta \approx 0.35$, B_t = 1T)

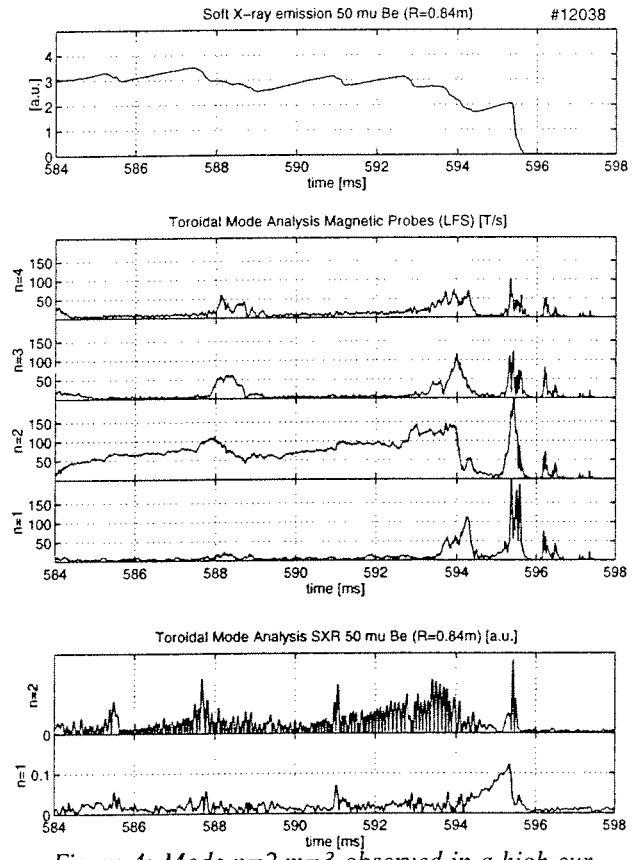

Figure 4: Mode n=2,m=3 observed in a high current discharge with improved confinement

"shoulders" near the q=1 surface and steep gradients towards the outside.

In contrast to the low current case, the plasma inductance decreases slightly.

3.Conditions for IOC

Up to now improved confinement was only observed with plasmas at elongations above 1.35. Low triangularity seems to be favourable as well as a slight tilt of the plasma. Both of these modifications reduce the extent of the plasma-wall interaction zone. This is consistent with the observation that wall conditions have a large effect on accessibility and quality of the improved confinement mode. Better improvement in confinement and faster transitions can be obtained whith low recycling walls. These conditions are

also favourable for H-modes in diverted TCV plasmas. A few discharges in a series of improved confinement shots switched to H-mode!

4.Conclusions

Transitions to an improved confinement regime for limited ohmically heated plasmas have been observed. Some of the observed features are very similar to those of the IOC regime observed in ASDEX in diverted discharges [3].

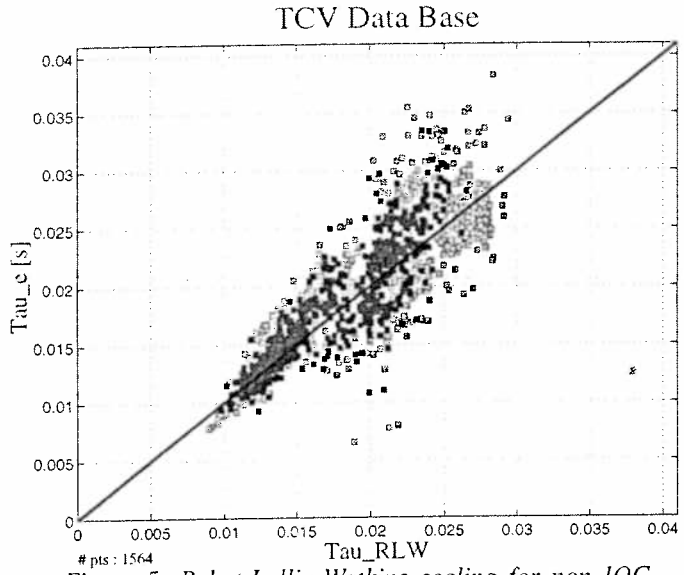

Figure 5: Rebut-Lallia-Watkins scaling for non IOC discharges (grey) and IOC dicharges (black)

The Rebut-Lallia-Watkins scaling was found to be appropriate for ohmic TCV discharges [4,5]. Plasmas with improved confinement do not deviate from RLW-scaling more than plasmas with "normal" confinement (figure 5). The RLW-scaling predicts the confinement time in the improved confinement mode reasonably well because of its strong power dependence (P^{-1}) and because of the reduced ohmic heating power in improved ohmic confinement.

High elongation and wall conditions with low recycling are favourable for reaching this regime. Profile changes, changes in internal inductance and changes in the sawtooth behaviour suggest a global change in the current density profile.

Acknowledgements

The authors acknowledge the support of the entire TCV team. This work was partly supported by the Swiss National Science Foundation.

References

[1] Hofmann, F. et al., Plasma Phys. Control. Fusion **36** (1994) B277

[2] Hofmann, F. et al., Poster P2.010, this conference

[3] Söldner, F.X. et al., Phys.Rev.Let. **61** (1988) 1105

[4] Nieswand, C. et al., 38th APS Meeting DPP. (1996) 6P38

[5] Weisen,H. et al., LRP571/97 (1997), submitted to Nuclear Fusion

Confinement Optimisation by Plasma Shaping on TCV

J.-M. Moret, R. Behn, S. Franke, F. Hofmann, H. Weisen

Centre de Recherches en Physique des Plasmas
Association EURATOM - Confédération Suisse
École Polytechnique Fédérale de Lausanne
CH-1015 Lausanne, Switzerland

Any improvement in the energy confinement time of a tokamak reactor may facilitate its access to ignition. TCV has the unique capability of creating a wide variety of plasma shapes and can therefore investigate to which extent an appropriate choice of the plasma shape can improve the energy confinement time. For simple shapes defined only by their elongation and triangularity, it has already been observed on TCV that the confinement properties of the plasma depend strongly on the shape [1,2]. This previous work has now been extended to include more complex shapes and higher elongations, in order firstly to test the applicability of the previously proposed explanation for the shape dependence of the confinement time and secondly to propose new shapes which offer a substantial gain on their confinement characteristics.

Experiments. TCV plasma shape is controlled by 16 independent poloidal coils. The present work is based on equilibria whose outer shape is defined by the analytical contour

$$(R, Z) = (R_0, Z_0) + a(\cos(\theta + \delta\sin\theta - \lambda\sin 2\theta), \kappa\sin\theta) \qquad (1)$$

where (R_0,Z_0) is the geometric axis position, a the minor radius, κ the elongation, δ the triangularity and λ the squareness. A negative λ tends to define a lozenge shape while a positive value gives the contour a rectangular shape. The studied shapes are divided in three sets: a systematic

	κ	δ	λ	q_a	$\bar{n}_e$ [10^{19}m^{-3}]
(κ,δ) scan	[1.0,1.9] × [-0.45,0.80]		0.00	[2.3,6.0] × [2.9,8.8]	
(δ,λ) scan	1.5	[-0.25,0.35] × [-0.10,0.30]		[2.3,5.1]	5.3
high κ	[1.9,2.6]	[0.30,0.50]	[0.05,0.25]	[2.5,3.9]	[2.7,8.5]

scan in the (κ,δ) plane at fixed λ; a systematic scan in the (δ,λ) plane at fixed κ; a set of highly elongated shapes for which κ and λ increase simultaneously at fixed δ. The value of the shape parameters κ,δ,λ comes from a fit of the contour (1) to the last closed flux surface (LCFS) de-

duced from the equilibrium reconstruction and may differ slightly from the usual definition based on the contact points of the circumscribed rectangle. For each shape a plasma current scan allows to separate the influence of the current itself, the safety factor, q_a, the shape and the ohmic input power, P_{oh}. All data points are obtained during stationary ohmic L-modes with R_0 = 0.88m, a = 0.25m, 1.43T, D_2. The confinement properties of these plasmas are quantified by the electron energy confinement time, $\tau_{Ee} = W_e/P_{oh}$, where the total electron thermal energy, W_e, is obtained by volume integration of Thomson scattering measurements at 10 to 25 spatial positions. At fixed q_a and fixed line average density, $\bar{n}_e$, the following variations in τ_{Ee} when the shape parameters are scanned are observed (fig. 1): (i) no significant modification with the elongation, even when comparing a circular plasma with an elongation as high as κ = 2.5; (ii) a marked degradation at positive triangularity compared with zero or slightly negative triangularity, which can reach a factor 3 at the highest densities; (iii) a substantial improvement for rectangular shapes when λ is increased from 0 to 0.3.

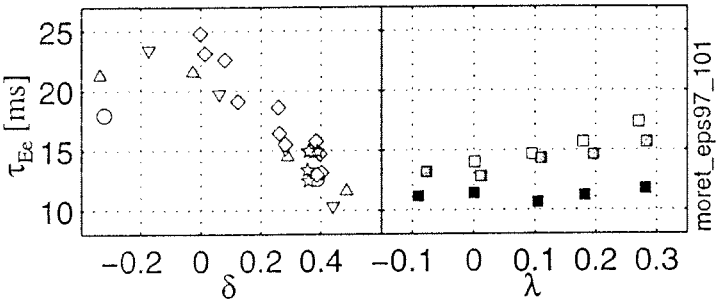

Fig. 1 Shape dependence of the electron energy confinement time for 3 < q_a < 4 and 4 × 10^{19} m^{-3} < n_e < 5.5 × 10^{19} m^{-3}. Left: from the (κ,δ) scan and high κ, ● κ = 1.2, ▲ κ = 1.37, ▼ κ = 1.55, ◆ κ = 1.72, ★ κ = 2.5. Right from the (δ,λ) scan, white δ = -0.18, grey δ = 0, black δ = 0.3.

Local transport. To understand these observations, it is necessary to determine the influence of the shape on the heat conduction, the main loss channel. A simplified radial power balance has then been established in which: (i) radiation losses, localised near the plasma edge, have been neglected; (ii) in the absence of a measurement of the ion temperature profile, ion and electron heat conduction fluxes are not separated. This yields the following heat flux equation:

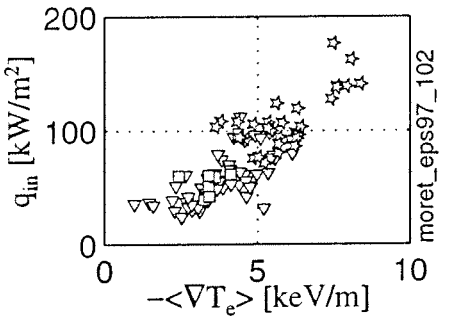

Fig. 2 Plot of the energy flux versus the temperature gradient in the region r/a = 0.8 for 5.5 × 10^{19} m^{-3} < n_e < 7 × 10^{19} m^{-3}: ▼ from the (κ,δ) scan, ■ from the (δ,λ) scan, ★ from high κ.

$$(q_{in} = -n\chi_{eff}\langle\nabla T_e\rangle),\ \chi_{eff} = \chi_e + \chi_i\frac{\nabla T_i}{\nabla T_e} \qquad (2)$$

where q_{in} is the input energy flux and $\langle\nabla T_e\rangle$ the electron temperature gradient averaged on a

flux surface. A plot of q_{in} versus $\langle \nabla T_e \rangle$ for a fixed density but a wide variety of plasma shapes indicates that the effective thermal diffusivity does not depend on the shape. There is however a non linear relationship between these parameters, indicating a dependence of χ_{eff} on $\langle \nabla T_e \rangle$. The second factor entering the conduction flux is the temperature gradient. A first direct consequence of shaping is a local modification of the flux surface separation and incidentally of the temperature gradient. To quantify this effect the latter can be written as

$$\nabla T = \frac{dT}{dr}\frac{dr}{d\psi}\nabla\psi \tag{3}$$

where ψ is the poloidal magnetic flux and r the distance from the magnetic axis measured at the outer midplane and normalised such that $r = a$ on the LCFS. This particular coordinate has been chosen instead of ψ because different ψ distribution can define the same geometry and because the Shafranov shift depends closely on the shape. Appropriate shaping creates large volume where the gradient geometrical factor, $\frac{dr}{d\psi}\nabla\psi$, is small and hence conduction losses reduced.

Shape Enhancement Factor. The gradient geometrical factor and the fact that the thermal diffusivity does not depend on the shape can be combined to quantify the influence of the geometry on the global energy confinement time. To do so, the confinement time of a shaped plasma is compared to that of cylindrical plasma (indexed o) with the same thermal conduction and the same input energy flux. It is then convinient to introduce a "Shape Enhancement Factor" (SEF) as the ratio of these two confinement times:

$$H_s = \frac{S_o \int_0^a n \int_r^a \frac{q_{in}}{n\chi}\frac{d\psi}{dr} \langle \nabla\psi \rangle^{-1} dr' dV}{S \int_0^a n \int_r^a \frac{q_{in}}{n\chi} dr' dV_o} \tag{4}$$

where S is the LCFS area. In the results presented here, the SEF has been computed using a flat

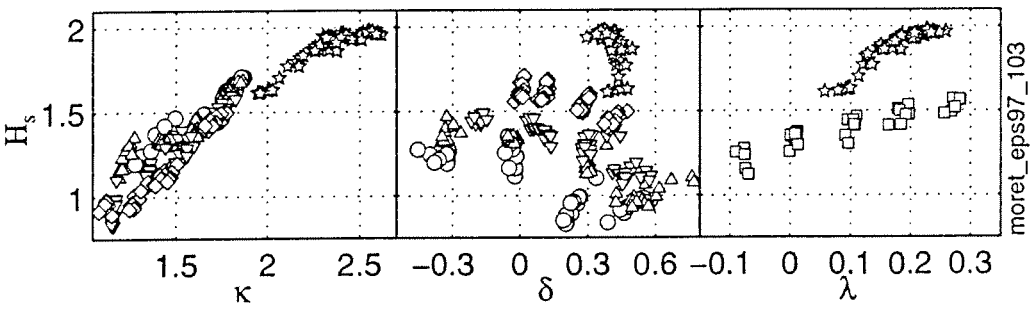

Fig. 3 Value of the Shape Enhancement Factor for different shapes. Left: from the (κ,δ) scan with ●▼▲◆ representing increasing δ and ★ from high κ. Middle: from the (κ,δ) scan with ●▼▲◆ representing increasing κ and ★ from high κ. Right: ■ from the (δ,λ) scan and ★ from high κ.

density profile and a canonic profile for $\frac{q_{in}}{n\chi}$, so that H_s depends only on the geometry via the ψ distribution. In the derivation of the expression for H_s, the thermal diffusivity was assumed independent of ∇T or $\langle \nabla T \rangle$. This hypothesis can be relaxed without noticeable modification in the H_s value [2]. Variation of the SEF with the three shape parameters κ,δ,λ is shown in figure 2. It increases continuously with κ but saturates at a limiting value of 2 for high elongation. It decreases markedly for high positive δ compared to its value around $\delta = 0$; computation on theoretical equilibria with very negative δ indicates that the SEF should reach a maximum for slightly negative values of δ; this remains to be experimentally verified. The SEF finally displays a substantial improvement for rectangular shapes with a large λ, typically 25% over the explored range. Obviously the variations in the SEF correspond to that observed in the energy confinement time. Thus dividing the confinement time by H_s should cancel the shape dependence. There remains however a decrease of τ_{Ee}/H_s when κ and δ increase, but this persisting variation can easily be interpreted as a heat flux degradation effect (fig. 3), $(P_{oh}/S)^{-0.5}$, since increase both in κ and δ are accompanied by an increase in P_{oh} [1,2].

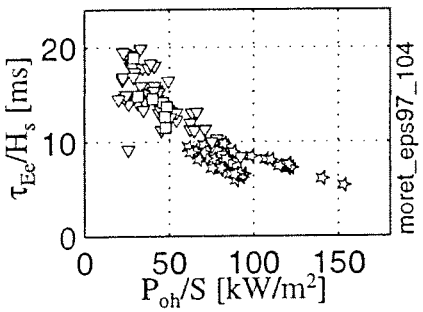

Fig. 4 Energy flux degradation of the corrected confinement time. Symbols and data selection as in fig. 2.

Conclusion. In summary, no influence of the plasma shape on the transport mechanism has been found for the explored shapes and operational regimes. Global energy confinement can however be considerably improved by plasma shaping, which by geometrical effects reduces the temperature gradient and the associated conduction losses. The formulation of this improvement in term of a Shape Enhancement Factor has proved to apply also to more complex shapes and to high elongations. It can therefore be safely used as a criterion for optimising the shape effects. Study of the influence of high order shape parameter, such as the squareness, shows that even if engineering or physical constraints may restrict the choice of the basic shape parameters, there remains room for a substantial gain in the confinement properties with an appropriate shaping.

This work was partially supported by the Fonds National Suisse pour la Recherche Scientifique.

[1] J.-M. Moret, S. Franke, H. Weisen et al., LRP 560/96, submitted for publication in Physical Review Letters.

[2] H. Weisen, J.-M. Moret, S. Franke et al., LRP 571/97, accepted for publication in Nuclear Fusion.

X-Ray measurements of MHD activity in shaped TCV plasmas.

I. Furno, H. Weisen, J.M. Moret, P. Blanchard and M. Anton*
Centre de Recherches en Physique des Plasmas, Association EURATOM-Confédération Suisse
EPFL,CH-1015 Lausanne, Switzerland
*present address: Max Planck Institut für Plasmaphysik, D-8046 Garching, Deutschland.

1 . Introduction

The ability of TCV to produce a wide variety of plasma shapes has allowed an investigation of MHD behaviour in a large number of limited ohmic L-mode discharges in which the elongation κ and the triangularity δ have been varied over a wide range: κ=1.1->2.5, δ=-0.3->0.7.
A 200 channel soft X-ray tomography system in conjuction with toroidally spaced soft X-ray diodes has been used to study the structure of internal disruptions and MHD modes. A strong reduction of sawtooth amplitude is observed as the plasma triangularity is decreased together with an increase in mode activity. The reduced sawtooth amplitudes are not correlated with any significant changes of the inversion radius and hence are not simply due to changes in current profiles; the inversion radius however is strongly correlated with the Spitzer conductivity profile and with the edge safety factor.

2 . Diagnostics

The soft X-ray tomography on TCV consists of ten cameras placed in a poloidal plane looking at the plasma through a curved Beryllium filter of 47 μm of thickness; each camera is equipped with a linear array detector of 20 photodiodes providing a total of 200 lines of sight and allowing a spatial resolution of about 3 cm. The acquisition frequency of the system is 10 kHz.
The line integrated signals are tomographically inverted using the Minimum Fisher Information method and the reconstructed poloidal emissivities are analyzed with the help of *Singular Value Decomposition* (SVD), allowing the determination of MHD mode structures and the sawtooth inversion radius [1].
The soft X-ray emissivity from the plasma is also monitored by four silicon photodiodes, equipped with a Beryllium filter of 50 μm thickness, placed at the top of the vessel and equally spaced in the toroidal direction. The viewing lines of these detectors cut the poloidal midplane ≅7 cm from the centre of the vessel in the direction of the major axis. The availability of these 4 photodiodes allows us to distinguish between n=1 or n=3 (by aliasing) and n=2 modes.

3 . MHD and sawtooth behaviour

The most important feature of shape on MHD behaviour is observed as the triangularity is changed. Shots at high triangularity are characterized by large sawtooth amplitude and low level MHD modes; as the triangularity is reduced the sawtooth activity decreases and the MHD modes become persistent (Fig. 1, top).

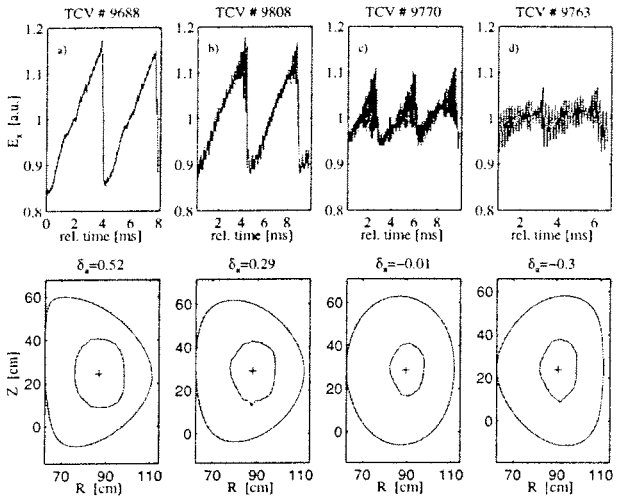

Fig.1. Raw X-Ray signals (top of the figure) with Sawtooth and Mirnov oscillations. Sawtooth inversion radius (bottom of the figure) and LCFS for four different triangularities. All discharges had $q_a=3.5$ $n_e=5.0\ 10^{19}\ m^{-3}$, $\kappa_a=1.4$.

The SVD analysis in conjunction with the toroidal Fourier analysis has allowed the identification of MHD mode structures.

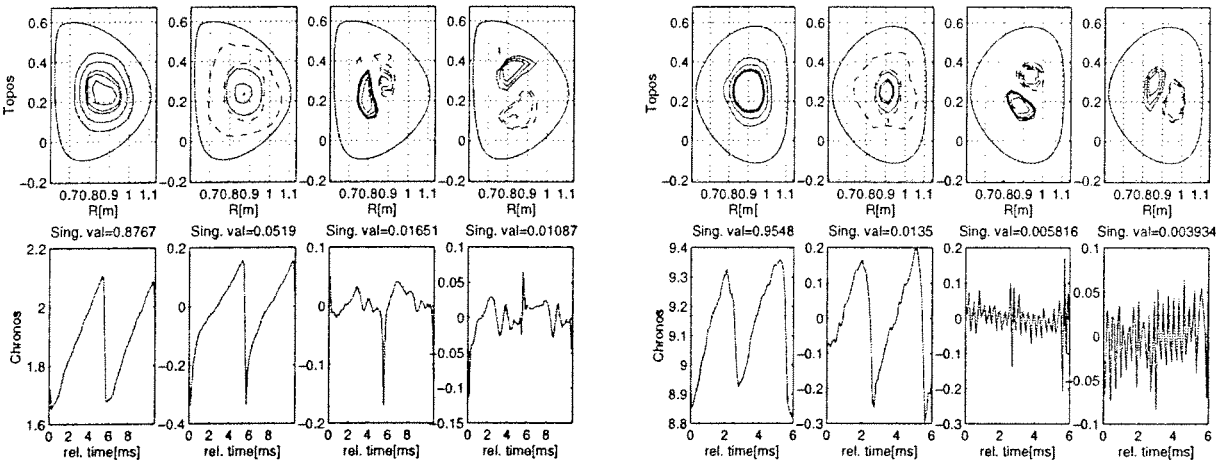

Fig. 2: SVD analysis of the shot 9688 (a) and 9763 (b). Contour plots of the different Topos are shown at the top of the figure with the LCFS; dotted lines correspond to negative value of the Topos. At the bottom the corresponding Chronos normalized to the sawtooth singular value are shown.

As can be seen in Fig. 2, for $\delta>0$ the MHD activity is mainly due to non-axisymmetric modes localized near the q= 1 surface. These modes, presumably tearing modes, are present only as brief precursors or postcursors of the sawtooth crash, being almost absent during the sawtooth

ramp. For $\delta<0$ MHD activity becomes continuous and appears as a rotating m=1/n=1 mode. The maximum of the mode amplitude is reached during the sawtooth crash and the rotation is in the direction of the electron diamagnetic drift. At very negative triangularity these modes can lead to a loss of confinement and cause disruptions by mode locking.

As the elongation is increased beyond 2 an m=2/n=2 locked or slowly rotating mode becomes important (Fig. 3), reaching maximum amplitude during the sawtooth crash. The amplitude of these mode increases with the elongation and, at fixed shape, increases as the edge safety factor is reduced. The presence of this mode is consistent with the observation of an m=3, n=2 mode in the soft X-ray emissivity and in the Mirnov probes during major disruptions in TCV [3-4].

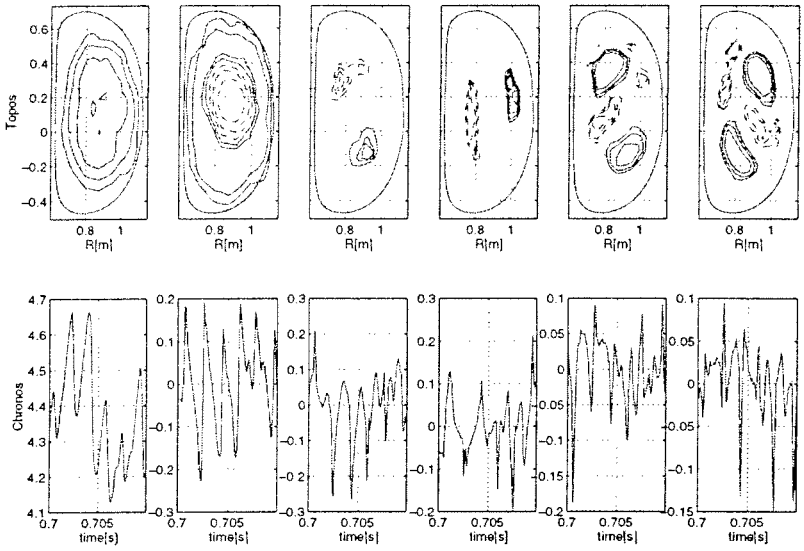

Fig. 3: SVD analysis of TCV SHOT# 11832 at t=0.7-0.71. The shot parameters are:I_p=0.7 MA, κ_{95}=2.38, δ_{95}=0.28. At the top of the figure, the Topos with the LCFS are shown together with the corresponding Chronos (bottom). Topos #3 and #4 show the normal 1/1 activity, while Topos #5 and #6 show the superposed slowly rotating 2/2 mode

The amplitude of the sawtooth crash varies strongly with triangularity, being largest at positive triangularity and sometimes vanishing at negative triangularity [2]. This behaviour can be explained by the fact that any reduction in the ohmic input power, caused either by reduction of current density (high q_a discharges) or by an improvement in energy confinement as observed for $\delta<0$, leads to a reduction of sawtooth reheat power. In Fig. 4 we see that plasmas with highest confinement times have lower ohmic heating power and hence small sawtooth amplitudes.

The sawtooth inversion radius, defined as $\rho_{inv}=(V_{inv}/V)^{1/2}$ where V_{inv} is the plasma volume inside the inversion contour, correlates very well with the cross sectional area averaged current density. This is shown in Fig. 5 where as abscissa we use the non-dimensional average current density $\langle j\rangle^*=\mu_0 R_0\langle j\rangle/B_T$; symbols refer to classes of δ_a showing that there is no intrinsic de-

pendence of the inversion radius on triangularity. This good correlation could be explained by assuming that the effect of sawtoothing is to flatten the current profile inside the inversion radius, preventing the current density from rising to a value higher than that corresponding to q≡1 for $r \leq r_{inv}$.

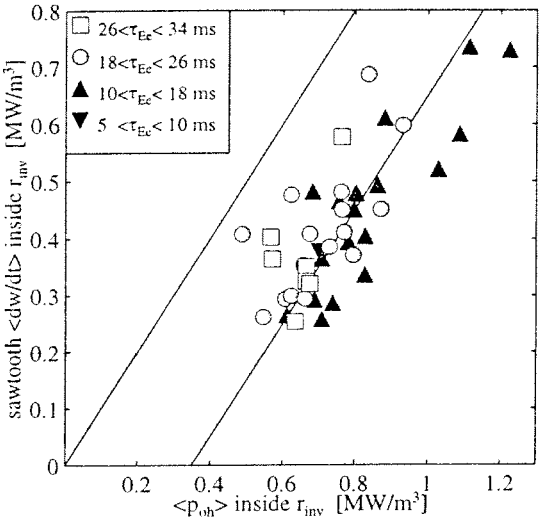

Fig. Sawtooth reheat power versus central ohmic heating power inside inversion radius for $n_e=6.3*10^{19}$ m^{-3}. The upper line corresponds to $\langle dw_0/dt\rangle_{inv}=\langle p_{oh}\rangle_{inv}$, the lower line to $\langle dw_0/dt\rangle_{inv}=\langle p_{oh}\rangle_{inv}-0.35$ MW/m^3. Symbols refer to classes of confinement time.

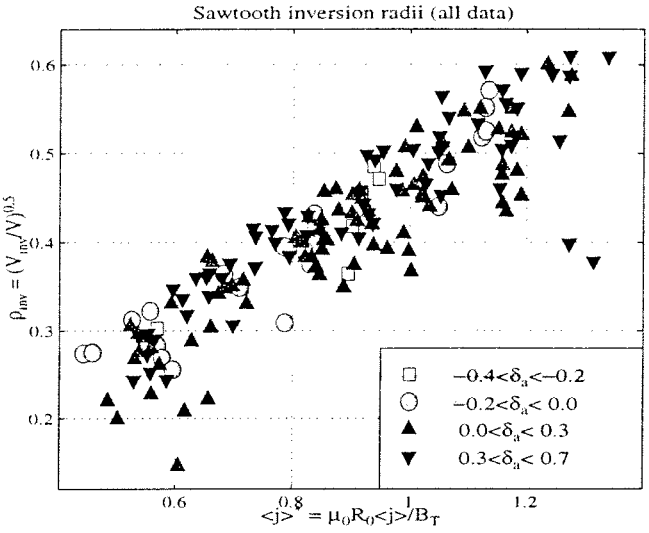

Fig. 5. Normalized sawtooth inversion radius versus non-dimensional average current density. Symbols refer to classes of triangularity.

The reduction of the ohmic input power with δ_a may explain, at least partly, the increase of mode activity. This reduction leads to lower edge electron temperatures [2], which may contribute to destabilizing resistive modes. High amplitude modes are unlikely to develop with Te(0.9a)>200 eV but are frequent at lower temperature. This suggests that the mode observed by X-ray tomography at the q=1 surface may be induced by mode coupling with m>1,n=1 which are destabilized near the plasma edge.

Acknowledgement

This work was partly funded by the Swiss National Funds for Scientific Research.

References

[1] M. Anton *et al, Plasma Phy. and Control. Fusion 38, 1849-1878 (1996).*

[2] H. Weisen *et al, Effect of plasma shape on confinement and MHD behaviour in TCV Tokamak* submitted for publication to Nuclear Fusion, available as LRP 571/97.

[3] O. Sauter *et al,* this conf.

[4] F. Hofmann *et al*, this conf.

Heating and Confinement Studies with ECRH in the TCV Tokamak

A.Pochelon, T.P.Goodman, M.Henderson, Z.A.Pietrzyk, M.Q.Tran, I.Furno, F.Hofmann, JP.Hogge, JM.Moret, F.Perthuisot, H.Reimerdes, O.Sauter, H.Weisen, S.Alberti, R.Behn, F.Bühlmann, S.Coda, M.J.Dutch, B.P.Duval, S.Franke, R.W.Harvey*, B.Joye, J.B.Lister, Y.Martin, P.Mandrin, Ch.Nieswand, R.A.Pitts, J.Rommers, W.van Toledo, G.Tonetti

Y.V.Esipchuk†, A.A.Martynov†, K.A.Razumova†, I.N.Roy†

Centre de Recherches en Physique des Plasmas, Ecole Polytechnique Fédérale de Lausanne, Association EURATOM-Confédération Suisse, CH-1015 Lausanne, Switzerland
†Kurchatov Institute of Atomic Energy, 123182 Moscow, RF
*CompX, Del Mar, Ca., USA

Introduction - ECRH experiments have recently started on the TCV tokamak with the use of 1 MW, X2 heating. The ECW system installation is continuing and will eventually provide 3 MW X2 and 1.5 MW X3 [1]. The study of the effects of different heating localization is possible using *1)* the mobile mirrors of the launcher, *2)* the large vertical room for displacing the plasma in the TCV vessel and *3)* the radial displacement of the cyclotron resonance with magnetic field. Initial studies of heating and confinement have concentrated mostly on close-to-circular plasmas to allow the largest variation of beam-plasma geometry and to allow comparison with earlier results on other machines - a necessary first step before investigating more strongly shaped plasmas. For TCV parameters (R = 0.89 m, a = 0.25 m, I_p < 1.2 MA), the nominal field of B = 1.44 T and the frequency of 82.7 GHz of X2 gyrotrons places the resonance position on the high-field side (HFS) of the magnetic axis (Δ=-0.16 to -0.2); while the frequency of 118GHz of X3 gyrotrons results in a slightly low-field side (LFS) resonance position.

Central MHD-activity - Different types of sawtooth activities are observed while scanning the safety factor q, the injected power P_{EC} or triangularity δ. The standard sequence observed when increasing q, P_{EC}, or decreasing δ, with a heat deposition close to q=1, starts from *1)* ohmic-like, normal sawteeth (NST), of the standard triangular shape, passing

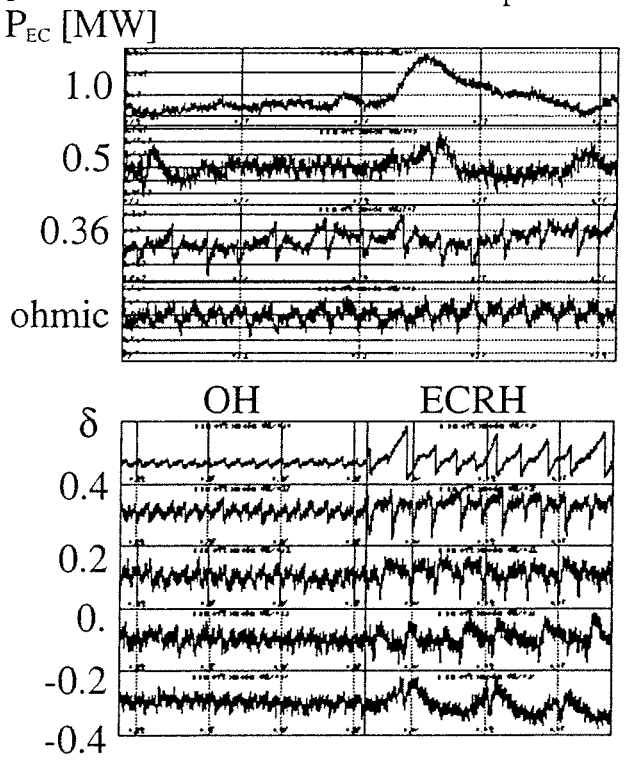

Fig.1 Change of central sawtooth activity in a a) power scan, b) triangularity scan

through *2)* saturated sawteeth (SST), where the temperature saturates after the fast reheat following the sawtooth crash and *3)* humpback sawteeth (HBST), earlier seen in ECCD experiments on T-10 [2] to *4)* complete substitution of sawtooth activity by a kind of "hilling activity" (HA), resembling HBST but where the crashes have completely disappeared. An example of these different types of sawteeth is shown in Fig. 1a) for a power scan and Fig. 1b) for a triangularity scan. A decrease of D_α emission during HBST and HA suggests improved particle confinement.

A study of the change of ST period and reheat after crash with heating close to or inside of q=1, has been performed by the three different swept deposition methods. Sweeping the plasma vertically through a fixed ECH beam keeps the incidence angle on the resonance constant but changes slightly the magnetic configuration. Sweeping the B-field at constant q is also non-stationary, but provides a sweep of the resonance location along the major radius. Whilst a sweep of the mirror angle θ in the poloidal plane produces a scan along the resonance in the vertical direction in a stationary magnetic configuration, albeit with a varying incidence angle on the resonance. For all three sweeps, a maximum of the ST period occurs when heating close to the ST inversion radius obtained from soft X-ray tomography, see Fig. 2 for the example of a vertical, z-sweep. The rate of reheating increases when heating inside of the inversion radius. Moving the deposition further towards the magnetic axis produces longer, giant ST of high, but strongly fluctuating, temperature.

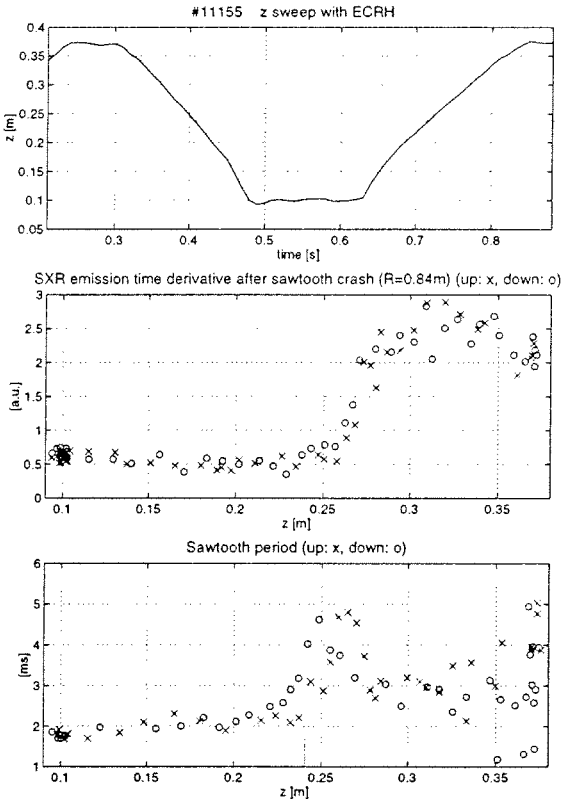

Fig. 2 Radial deposition z-sweep showing initial sawtooth reheat slope and sawtooth period maximal close to q=1

The saturation of the electron temperature after the fast reheat occurring with deposition between q=1 and the axis as suggested by soft X-ray emission signals, has been confirmed by Thomson scattering measurements. The saturation seems to be linked with the appearance of n=2 mode activity on q=1, measured both from magnetic probes (Fig. 3) and from soft X-rays, prior to the usual (1,1) mode. When the (1,1) mode vanishes for central enough heating, the central pressure rises again in the final stage of the sawtooth development, producing giant sawteeth.

Optimization of confinement versus localization (B,q) and versus (P,n_e) - An initial confinement study was carried out on a small target plasma placed in front of the launcher with quasi-horizontal launch in order to minimize effects related to the launch geometry with regard to refraction (θ=18°, z=38, κ=1.31, δ=0.15). Scan domains were: 1.32<B<1.45T, representing a 20% radial displacement of the resonance around q=1;

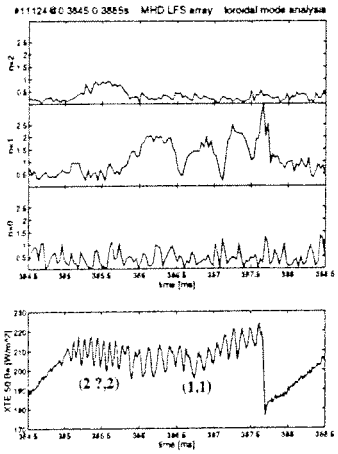

Fig. 3 Central temperature saturation and n = 2,1,0 activity during a single sawtooth.

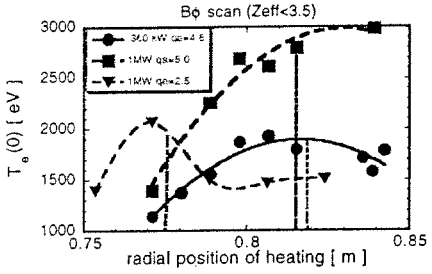

a) electron temperature

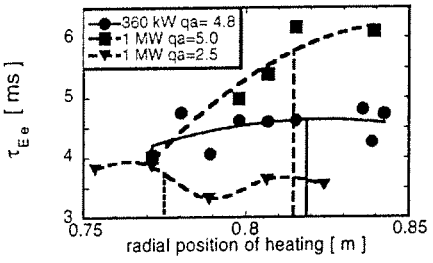

b) confinement time τ_{Ee}

Fig. 4 Radial deposition during a B-field scan: both a) and b) have the q=1 position indicated.

$1.5 \times 10^{19}m^{-3} < n_{eo} <$ over-dense (X2 cut-off at 4.25); $2.2<q<6$; $P_{EC} \leq 1MW$. This power led to a ratio P_{tot}/P_{oh} during ECRH from 3 to 14 in the q-scan for 1MW power injection.

In a B-field scan, for high-q (~5) moderate-power (0.5MW) shots, the plasma temperature response depends strongly on the radial location of the power deposition relative to the q=1 surface. The *central* electron temperature is maximum with deposition close to (but perhaps slightly outside) the q=1 surface (Fig. 4a) as determined from the sawtooth inversion radius from the soft X-ray camera data. The central temperature decreases slightly as the deposition location moves inside the q=1 surface but again rises as the deposition location moves further towards the center. The electron confinement time does not show such a strong dependence on localization during this scan; although, low-q high-power shots show an increase (as with T_e) for this location close to q=1 (Fig. 4b). As a function of the safety factor q, the dependence is much stronger, with τ_{Ee} increasing with q, maximizing at q~5.5 and dropping beyond q~6 (Fig. 5).

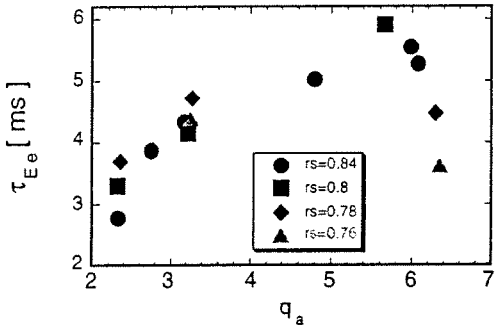

Fig. 5 τ_{Ee} versus q, for different deposition radii in a Bφ scan.

The power degradation exponent α_P, ($\tau_{Ee} \sim P^{-\alpha_P}$), is weaker than usually expected: $-0.5<\alpha_P<-0.4$, as measured for q=5 at $n_{eo}=2$ and $3\times10^{19}m^{-3}$ (see Fig. 6), and at q=2.5 for a density close to $2\times10^{19}m^{-3}$. This low confinement degradation may originate from the impact of heating on profiles and MHD-activity (in particular the sawtooth period) during slightly off-axis heating. When considering only power scans up to 0.5MW, higher degradation exponents are obtained. This yields similar power and density exponents as obtained earlier in T-10 electron cyclotron heating [3]. At the opening of the vessel following the campaign, a verification of the launchers revealed that one of the launchers had a non-zero toroidal angle, thus some features of the heating results, with $P_{EC}>500kW$, may contain an ECCD component.

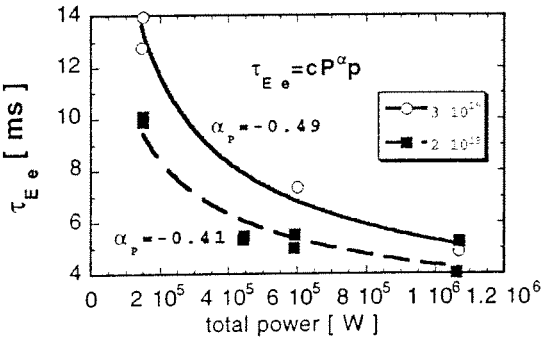

Fig. 6 τ_{Ee} power degradation for two densities, q=5

Transport simulations of TCV discharges - ECRH heated discharges have been simulated using the ASTRA transport code. The T-10 transport model in the ASTRA code was benchmarked against TCV ohmic data in order to reproduce the central temperature evolution. In the ohmic regime, the measured temperature profiles $T_e(r)$ of TCV are well described (accuracy ±10%) by the T-10 model (i.e. similar electron transport and confinement laws can be used). Early discharges had q=3.1, κ=1.26, differing oblique beam incidence angles on the resonance ($15^o<\theta<45^o$) to correspond to the z-sweep and static plasmas with saturated sawteeth when heating inside q=1. To simulate correctly the measured central temperature during ECRH, it was necessary to use an absorption efficiency factor k~0.65<1 (where $P_{ab} = k\,P_{input}$ or more correctly, $P_{ab} = k\,P_{ab}^{TORAY}$), as in other ECRH experiments [4]. Thus, under the condition $P_{ab} = 0.65\,P_{in}$, the T-10 model correctly describes (in the stationary case) not only values and profiles of $T_e(r)$ and $n_e(r)$ but also the temperature responses for different power deposition profiles. Simulating more recent shots, with high q~6, κ=1.32, $n_{eo}=2\times10^{19}m^{-3}$ in quasi-horizontal launch ($\theta=18^o$), where T_{eo}=3keV was obtained with 0.5MW, a higher k-factor, close to unity was appropriate.

Conclusions - Heating effects, MHD-activity and to a lesser degree confinement, are shown to depend strongly on the localization of the EC power deposition location. This has been shown in sweeps and scans of mirror angle, vertical plasma position and magnetic field. Sawteeth and mode activity are stabilized/de stabilized depending on the location of the power deposition relative to the q=1 surface. Dramatic changes in central temperatures occur when heating is close to q=1 or towards the magnetic axis. A similar trend, though weaker, exists for confinement time. Confinement increases significantly with q, culminating at q~5-6, before dropping at higher values. The effect of q on confinement is more dramatic than the effect of B-field variation, displacing the resonance in the range of ±3-4cm around q=1 surface. The power degradation exponent has a value between -0.4 and -0.5, a weaker degradation than generally expected, which may originate from effects improving confinement, like sawteeth stabilization or reduced shear due to the slightly off-axis deposition.

This work is partially supported by the Fonds National Suisse de la Recherche Scientifique.

References

[1] T.P Goodman et al., 19th SOFT, Lisbon, Sept. 1996; A. Pochelon et al., 20th EPS Conf on contr. Fus. and Plasma Phys., Vol. 17C, Part III (1993)1029;
and T.P Goodman et al., Proc. EC-10 Conf., presented by M.Q. Tran, Ameland 1997

[2] D.A Kislov et al., 22nd EPS Conf on contr. Fus. and Plasma Phys., Vol. 19C, Part I (1995) 369

[3] Y. Esipchuk et al., J. Moscow Phys. Soc. 1(1991)119 and ITER-IL-PH-4-9-5-10(1991)

[4] V.V. Alikaeev et al., Proc. 10th Int. Conf. on Plasma Phys. and cont. nucl. Fus., Vol I (1985) 419; and V.V. Abrakov et al. Nucl. Fus. 37 (1997) 233

Statistical Study of TCV disruptivity and H-mode Accessibility

Y. Martin, Ch Deschenaux, J.B. Lister, A. Pochelon

Centre de Recherches en Physique des Plasmas,
Association EURATOM - Confédération Suisse,
Ecole Polytechnique Fédérale de Lausanne, CH-1015 Lausanne, Switzerland

INTRODUCTION

Optimising tokamak operation consists of finding a path, in a multidimensional parameter space, which leads to the desired plasma characteristics and avoids hazardous regions. Typically the desirable regions are the domain where an L-mode to H-mode transition can occur, and then, in the H-mode, where ELMs and the required high density can be maintained. The regions to avoid are those with a high rate of disruptivity. On TCV, learning the safe and successful paths is achieved empirically. This will no longer be possible in a machine like ITER, since only a small percentage of disrupted discharges will be tolerable. An *a priori* knowledge of the hazardous regions in ITER is therefore mandatory. This paper presents the results of a statistical analysis of the occurrence of disruptions in TCV.

For the H-mode accessibility, it is usually admitted that a minimum auxiliary power is required, and that this power threshold depends on some plasma parameters. On TCV, since the H-mode was achieved with Ohmic heating only, such a power threshold can not be determined. Plasma shape, current and densities as well as the vacuum vessel conditioning are known to play a role in the H-mode accessibility. Discriminant analysis, a powerful statistical method, has been used to estimate a probability of being close to an L-mode to H-mode (LH) transition, which could be used to guide the plasma discharge towards the LH transition, with the help of an advanced and intelligent control system.

PLASMA DISRUPTIVITY IN TCV

In order to quantify the disruption rate in TCV, we have defined the disruptivity as the number of disruptions observed in a multidimensional cell of the operational domain, divided by the total plasma operation time spent in that cell. This latter time is provided by a database containing time slices taken every 50 ms in every plasma discharges produced over more than two years of operation, a total of over 60'000 time slices. The disruptions have been visually

classified according to their operational context, such as during an L-mode or H-mode phase or in the presence of locking modes, etc. This allows us to analyse the disruptivity in different contexts separately and also to remove disruptions provoked by technical failures or feedback control experiments, which have nothing to do with the underlying physics of disruptions. The aim of such an approach is to identify the high disruptivity zones without *a priori* knowledge. For instance, the q=2 limit naturally emerges from the analysis as a hard limit, with only a slight increase in disruptivity for 2<q<3.

To answer the question whether the Greenwald density limit is a strong limit or not, we plot the disruptivity in the Greenwald diagram for 4 different contexts (fig 1). In the stationary case, in L-mode or H-mode or soon after a HL transition, the Greenwald limit (G=1) is not exceeded. However, the disruptivity does not increase with the Greenwald parameter (G). This limit then appears like a soft limit for the low currents in L-mode, in the sense that the plasma itself avoids going to higher density, but without disrupting. For higher plasma current values, the disruptivity simply increases with the plasma density, not with G. In H-mode plasmas, the disruptivity also increases with the density with only a weak dependence on the Greenwald parameter (Ip/a^2). During the current decay phase, the limit is exceeded, but with a high disruptivity. In this case the Greenwald density limit appears as a strong limit.

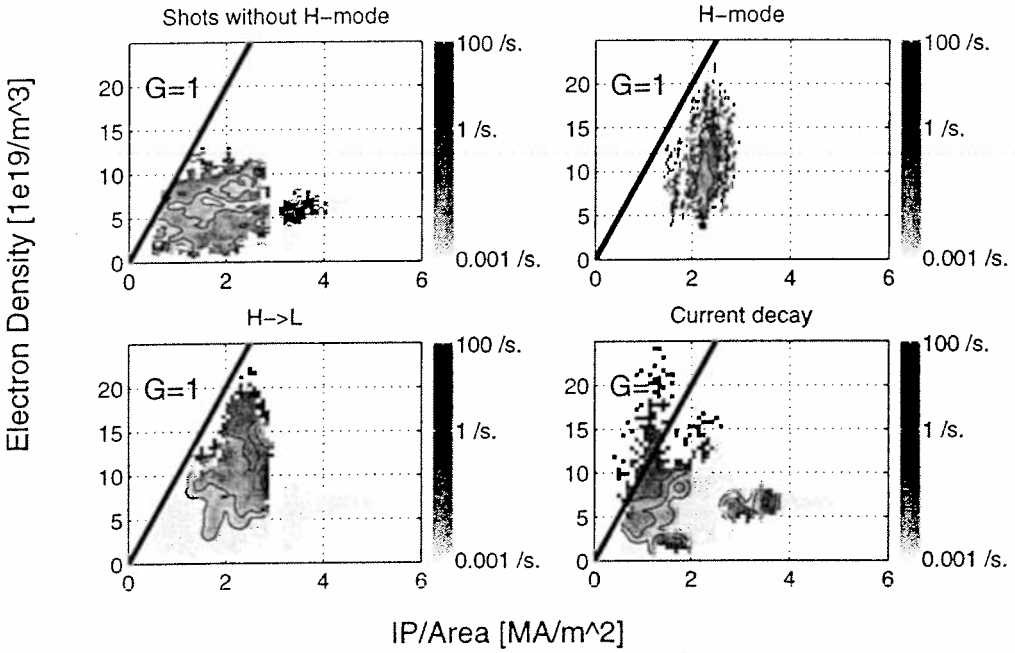

Fig 1: Disruptivity at the Greenwald density limit in different contexts

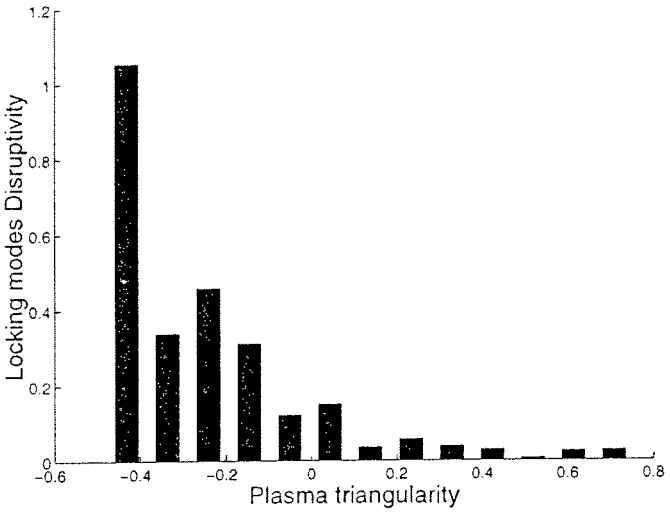

Fig 2: Disruptivity due to locking modes decreases with the triangularity

Although no clear dependence on the plasma shape is observed when all disruptions are taken together, either in a Hugill or li:q diagram, the disruptions due to locking modes are found to occur mainly at low triangularity, as shown in Fig. 2. This decrease of disruptivity at high positive triangularity is commonly used on TCV to cross q=3. For instance, even if the desired final plasma has a negative triangularity, its formation goes through a high triangularity phase (δ>0.2). With such a formation path, we performed 180 similar shots, one every morning, with a disruption rate lower than 1 %.

H-MODE ACCESSIBILITY

L-mode to H-mode transitions have been observed in TCV in a wide variety of ohmically heated plasma configurations (limited, single null, double null), plasma shapes (triagularity, elongation, gaps, ...), plasma currents, plasma densities and magnetic fields. Initially, the vacuum vessel conditioning appeared to play an important role in the reproducibility of the H-mode access. Since physics explanations of the effect of the conditioning remain unclear, a statistical approach, discriminant analysis, has been chosen, with the aim of extracting those parameters which are important for characterising the closeness to the LH transition.

Discriminant analysis consists of a multidimensional (R^n) coordinate transformation which minimises the intercorrelation between data groups while maximising the intracorrelation within a data group. In the case of a discrimination between two groups of data, only one variable, called the classification variable, is necessary to reveal the separation, if any. From that new variable, we define a probability of belonging to one or to the other of the two groups.

We calculated the classification variable, as well as the associated probability for two groups of data. One contains the time slices in L-mode before the transition and the other contains the time slices taken right at the LH transition. In a first step, the input parameters were the

plasma shape, current and density. This set of input parameters did not lead to a clear classification variable. We had to include the Ohmic power, the plasma temperature and a measure of the gas flux inside the machine to obtain a good enough classification variable, as shown in Fig. 3. The necessity of using this latter variable indicates the importance of the recycling on the H-mode accessibility.

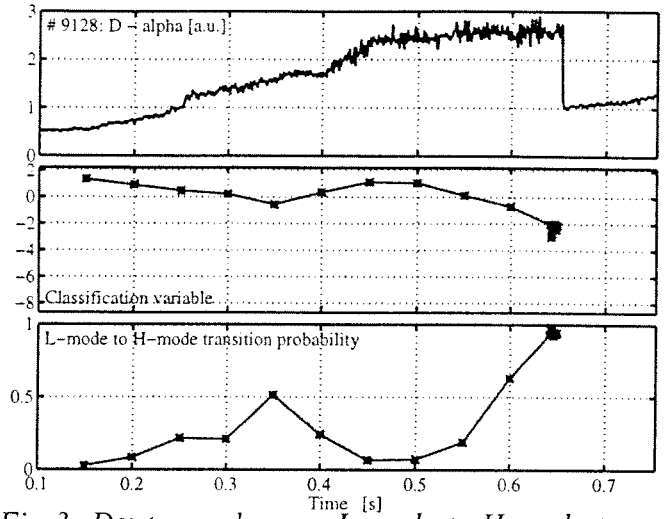

Fig 3: Dα trace shows a L-mode to H-mode transition, the discriminant variable and the associated probability reveals the imminence of the transition by the increase of the transition probability

Figure 4 shows the discriminant analysis results between L-mode and ELM free H-mode time slices, with the same input parameters. The probability curve clearly shows that a predictor can be easily calculated in this case.

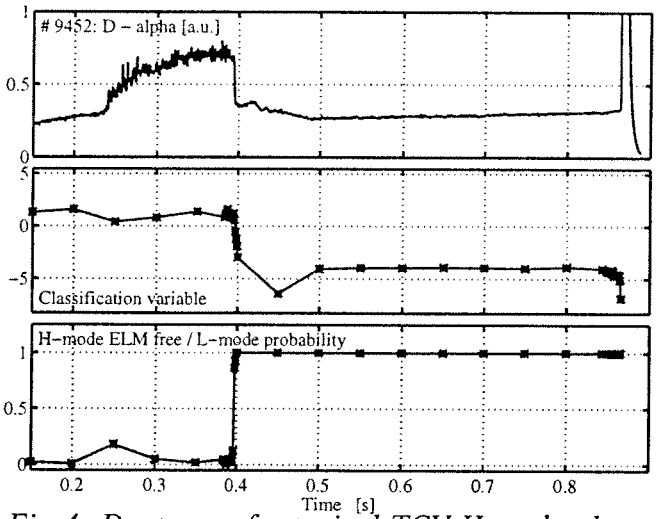

Fig 4: Dα trace of a typical TCV H-mode plasma, the discriminant variable and the associated probability showing the prediction to be in the H-mode

CONCLUSIONS

The disruptivity analysis reveals the importance of the plasma shaping during its formation in order to avoid disruptions due to locking modes. The Greenwald limit does not appear as a strong limit during the stationary phases.

Resulting from a discriminant analysis, a linear combination of plasma parameters, including information about the wall recycling, gives a probability of LH transition which is verified to increase and reach unity as the transition is approached.

ACKNOWLEDGEMENT

This work was partly supported by the Fonds National Suisse de la Recherche Scientifique.

Toroidally Asymmetric ELM Precursor Oscillations in the TCV Tokamak

H. Reimerdes, A. Pochelon, W. Suttrop†, Ph. Guittienne, H. Weisen

Centre de Recherches en Physique des Plasmas, Ecole Polytechnique Fédérale de Lausanne, Association EURATOM - Confédération Suisse, CH-1015 Lausanne

†Max-Planck Institut für Plasmaphysik, IPP - EURATOM Association, D-85748 Garching

Introduction

In TCV (R=0.89 m, a=0.25 m, I_p<1.2 MA, B_ϕ<1.5 T) ohmic H-modes have been obtained in diverted single-null (SND), double-null (DND), and elongated limited plasma configurations. In ELM-free H-modes the particle density rises continously until the discharge usually terminates with a high density disruption. Quasi-stationary H-modes have been obtained in the presence of ELMs. The observed ELM spectrum is continuous and ranges from clearly identifiable *type III ELMs* to low frequency, *large ELMs* [1]. The necessity of ELMs for particle control of H-mode plasmas while causing high peak-power loads on strike points makes the control of their level and nature desirable and motivates the study of the underlying MHD-instability.

Prior to ELMs in TCV coherent magnetic oscillations, that indicate a rapidly growing MHD instability, have been observed. The structure of these precursor oscillation is investigated with TCV's Mirnov probe arrays. In particular an observed toroidal asymmetry in the growth of the instability has to be explained.

Mirnov Probes on TCV

Toroidal and poloidal arrays of magnetic pick-up coils, measuring the poloidal magnetic field, have been installed inside TCV's vaccum vessel. For high-n mode analysis there are two complete toroidal arrays of 16 and 8 equally spaced probes, located on the equatorial low field side (LFS) and high field side (HFS) respectively. Poloidal arrays each with 38 probes were installed in 4 equidistant sectors. Data can be sampled up to a rate of 1 MHz. To maximize the signal amplitude, in spite of multipole field decay, toroidal and poloidal measurements have been performed on two different plasma configurations. For toroidal measurements a single null upper divertor (SNU) plasma on the midplane (z=0), allowing a minimal distance of down to 5 cm on the HFS and 7.5 cm on the LFS between the plasma edge and the toroidal array, is investigated (Fig. 1a). To allow maximum poloidal phase information the poloidal measurements have been performed on SNU plasmas, which were moved as close to the bottom as was possible during H-mode. A minimum distance of 10 cm to the probes at the bottom of the vessel has been achieved (Fig. 1b).

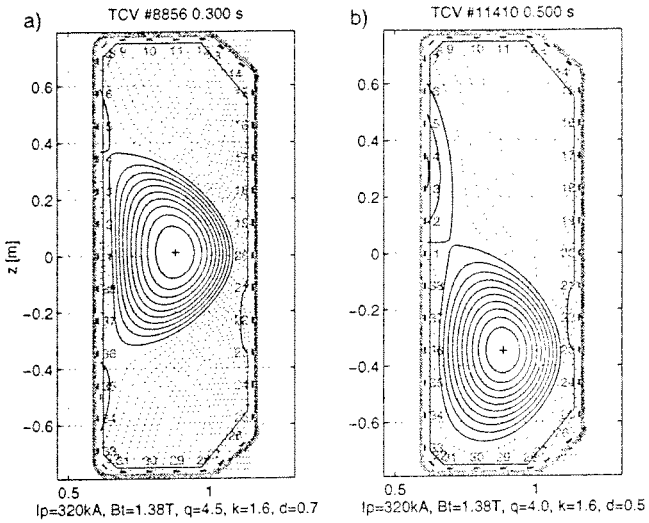

Figure 1: Poloidal cross section showing the position of the magnetic probes and the plasma configurations used: a) SNU configuration for toroidal mode number analysis. The toroidal arrays are located in the equatorial plane corresponding to positions 1 (HFS) and 20 (LFS). b) SNU configuration for poloidal mode number analysis.

Toroidal Measurements

The ELMs obtained in the discharges with fast toroidal measurements have caused a moderate particle loss of 2-4% and an energy loss of 2-6% of the total plasma content, which are typical figures for type III ELMs in TCV. Their repetition frequencies range from 120-300 Hz. For many ELMs a coherent precursor oscillation has been detected several 100 μs before the onset of the enhanced particle transport phase corresponding to the rise of the D_α-signal. The precursor is first detected on the LFS where it's amplitude is generally higher than on the HFS, even though the distance between probes and plasma is greater. The instability first develops at a toroidally localized position (Fig. 2). This precursor then grows both in amplitude and toroidal extent with a typical growth time of $\tau_{prec} = 50\,\mu$s. At the same time the frequency f_{prec} decreases from typically 120 to 70 kHz. When the precursor encompasses the whole toroidal circumference, the increased transport of energy and particles begins. The D_α signal increases rapidly, the magnetic oscillations lose their coherence while the fluctuation amplitude strongly rises. Due to the toroidal rotation of the precursor, measurements with a toroidally fixed probe show characteristics of beating as has been observed on other experiments [2,3].

The spatial measurements of $\dot{B}_\theta$ have been expanded into a Fourier series yielding toroidal mode numbers of $n = 0 \ldots 8$. It is clearly seen that the precursor consists of high n=5-8, predominantly 7 and 8, components (Fig. 2), but spatial aliasing could mask higher mode numbers such as 9 or 10. The amplitude of the n=8 component shows an oscillation with the precursor frequency due to the missing phase information at the Nyquist wave number. It is remarkable that a similar oscillation is also observed on lower n mode amplitudes.

There are several possible reasons for this toroidal asymmetry. For example the presence of two modes with Δn=1 show a spatial beating, that corresponds to a toroidal envelope of n=1. Nevertheless that does not explain either the oscillating amplitude of A_n for $n \leq 7$ or the existence of more than two toroidal mode components of the precursor.

A toroidal localization of an n=8 mode can explain these observations. Assuming a

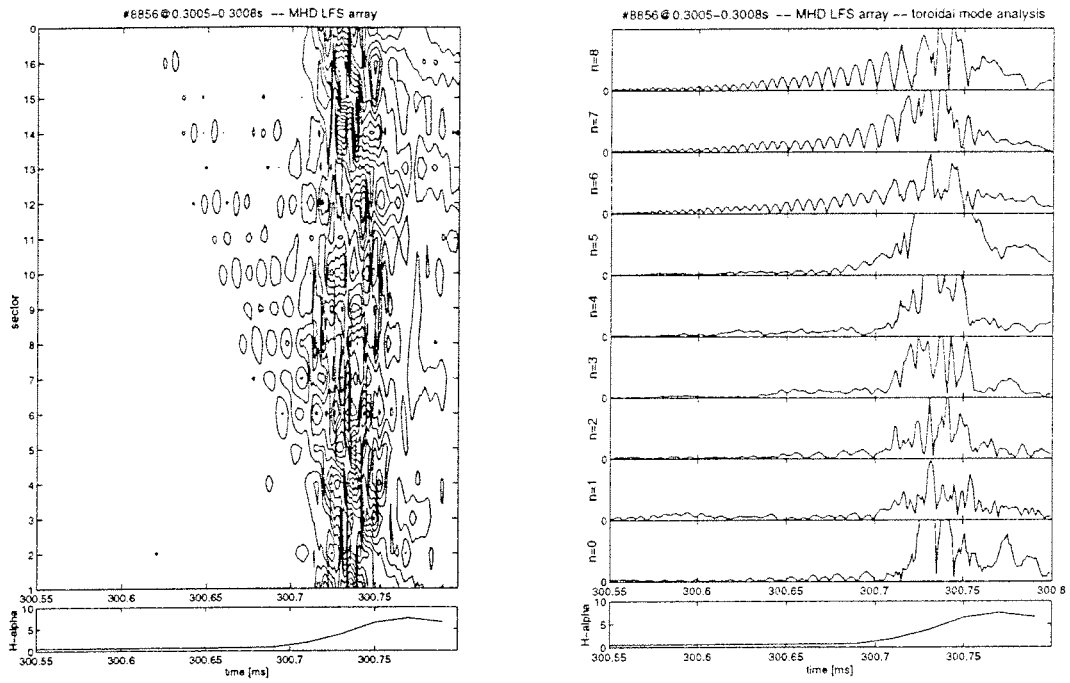

Figure 2: ELM-precursor oscillations seen with the toroidal array on the LFS. Left: Contour lines of $\dot{B}_\theta$ show the toroidally localized onset of the precursor. Right: Amplitude of the n=5-8 components grow before the beginning of the transport phase determined by the D_α-signal, which is shown below.

Gaussian toroidal weight of the amplitude of the pertubation field

$$\dot{B}(\phi,t) = A(t) \cdot e^{-\frac{1}{2}\frac{(\phi-\phi_{max})^2}{\sigma_\phi^2}} \cdot \sin(8\phi - \phi_0) \qquad (1)$$

the expected mode spectra show approximately a convolution of the n=8 spectrum with a Gaussian of half width $\sigma_n = 1/\sigma_\phi$. This is consistent with the observed mode spectrum (Fig. 2) and explains the oscillation of the amplitudes of $n \neq 8$.
Since the toroidally localized onset of the precursor differs for different ELMs, a localization due to errors in the measurements (i.e. hardware misalignment, gains) and a triggering of the ELM due to an asymmetry of the TCV assembly can be excluded.

Poloidal measurements

The ELMs obtained during discharges in the configuration shown in Fig. 1b) caused a higher particle loss of 4-7% and high energy losses of up to 11% of the total energy content, which is typical for *large ELMs*. The repetition frequency varied from 80-200 Hz. The probes on the LFS show coherent precursor oscillations with a frequency of $f_{prec} \approx$ 50 kHz and a typical growth time of $\tau_{prec} \approx 50$ μs. The observed local mode number of the precursor oscillation $m_{local} = \Delta\phi/\Delta\theta$ shows a dependence on the poloidal angle θ. The poloidal spacing of the probes limits the resolution ($m_{Ny} = \pi/\Delta\theta_{probes}$). Both vary strongly with the poloidal angle from $m_{Ny} \approx 8$ to $\gg 20$. If we assume a poloidally constant local

mode number $m_{local} = n \cdot q$ above the Nyquist mode number, the mode detected by aliasing would also vary with θ. Therefore the poloidal observations are consistent with high poloidal mode number of m≈16-20, but are, due to small signal amplitude, not unambiguous.

Conclusion

TCV ELMs believed to be type III ELMs and large ELMs both show magnetic precursor oscillations. Both precursors are strongly localized on the LFS. They both show similar growth rates and frequencies, which are in the range of values found for type III precursors on ASDEX-Upgrade [2] confirming the identification of TCV's type III ELMs and suggesting that TCV's *large ELMs* are large *type III ELMs*.
A toroidal mode analysis reveals high toroidal mode numbers. High n and a strong localization on the bad-curvature side support a ballooning-like instability as has previously been proposed for ELMs in various experiments [4]. The onset of the precursor is toroidally localized. Since asymmetries in the machine have been ruled out as a cause, this asymmetry must be intrinsic. A possible cause could be a low-n resistive mode located in the high pressure gradient region close to the plasma edge. It has been shown [5] that ideal ballooning modes are less stable on flux surfaces close to a magnetic island. A bunching of field lines close to the x-point can reduce the stabilizing shear and pressure gradients are enhanced near the island. This could give rise to a localized high n instability as has been observed prior to high-β disruptions in TFTR [6]. Weak low n mode activity has been observed, but a correlation between its phase and the onset of the precursor could not be retrieved.
The localized instability itself does not significantly enhance the radial transport over the separatrix. It is its encompassing of the entire toroidal circumference, that seems to be linked to the typical loss of particles and energy.

Acknowledgments

This work was partly funded by the Fond National Suisse de la Recherche Scientifique. The authors like to acknowledge the help of G. Tonetti.

References

[1] H. Weisen et al., Plasma Phys Control. Fusion **38** (1996) 1137.
[2] T. Kass et al., this conference.
[3] R. J. Buttery et al., Proc. 22nd EPS Conf. in Bournemouth 1995, Vol III p273.
[4] H. Zohm, Plasma Phys. Control. Fusion **38** (1996) 105.
[5] C. C. Hegna and J. D. Callen, Phys. Fluids B, **4** (1992) 3031.
[6] E. D. Fredrickson et al., Phys. Plasmas **2** (1995) 4216.

Comparison of the CREATE-L Plasma Response Model With Experiments on TCV

P. Vyas[1], F. Villone[2], J.B. Lister[1], R. Albanese[3]

[1] CRPP-EPFL, Association EURATOM-Suisse, CH-1015 Lausanne, Switzerland
[2] Associazione EURATOM/ENEA/CREATE, Dip. di Ing. Industriale,Univ. di Cassino, I-03043, Cassino (FR), Italy

[3] Associazione EURATOM/ENEA/CREATE, DIEMA, Univ. di Reggio Calabria, I-89125, Reggio Calabria, Italy

Abstract Experiments have been performed on the TCV tokamak to evaluate the response of Ohmic, L-Mode, limited and diverted plasmas to changes in the poloidal field coil voltages. The resulting closed loop plasma responses have been compared with the CREATE-L linearized MHD equilibrium model of TCV. The simulated responses show excellent agreement with the experiments in both the time and frequency domains. Tests with models derived using different assumptions indicate that the underlying physical assumptions of the nominal model are appropriate.

Introduction The CREATE-L plasma response model is derived by linearizing the equilibrium equation and Ohm's law in the active and passive conductors and in the plasma. In this model, the plasma is assumed to be in permanent MHD equilibrium and the plasma current density profile is kept fixed, whereas the total plasma current is allowed to vary. The boundary and magnetic axis fluxes are also allowed to vary. The model can be used to predict the plasma current, shape and position response to voltages applied to control coils and is being used to design the ITER Poloidal Field Coil control system. In ITER only small margins in power, coil voltages and currents are available for plasma shape control and it is important that the model used to design the feedback control loop should be accurate.

TCV discharges were fully simulated by the CREATE-L model, including details of the 18 external poloidal field coils, their power supplies, the passive vessel structure, the poloidal magnetic field and flux sensors as well as the plasma equilibrium for the particular discharges used. Selected limited and diverted plasmas have been examined.

This paper describes the experimental details of the comparisons and presents the results of comparisons for various plasma parameters. Models based on different physical assumptions are also compared.

Experimental set-up Experiments were performed on two plasma equilibria. An up-down symmetric, centred, limited L-mode configuration (κ=1.44, δ=0.3, I_p=200kA, q_a=5.5) and an L-mode, noncentred, single-null diverted plasma (κ=1.44, δ=0.38, I_p=200kA, q_a=7.3). The

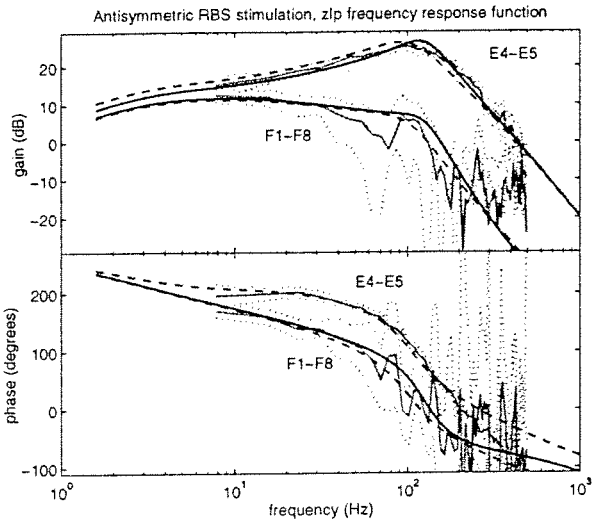

Fig.1 Response of limited plasma to antisymmetric RBS stimulation for expt. (light solid with dotted confidence bounds), CREATE-L (dark solid), and RCDM (dashed)

plasma position and shape responses were excited by adding stimulation voltages to the poloidal field control coils. Responses to 50ms square pulses were examined in the time domain to provide a simple visual test of the model-experiment agreement. Random binary sequences (RBS) were applied to provide data for spectral analysis for frequency domain comparison over a wider bandwidth.

The symmetry of the limited plasma was exploited to improve the signal to noise ratio. Up-down antisymmetric coil-pair stimulation was used to excite the plasma vertical position, and symmetric pair excitation was used to excite other parameters. Single coil excitation was used for the diverted plasma.

All experiments were performed in closed loop with feedback on five control variables constructed from linear combinations of poloidal flux, field and poloidal field coil currents. These were the vertical flux imbalance (P_VERT) which provides a measure of radial position; the outboard field curvature (TRI_OUT) and in the inboard field curvature (TRI_IN) which together provide a measure of plasma elongation and triangularity; the vertical position current moment (zI_p); and the plasma current (I_p). An additional parameter related to the radial current moment (PSI_R) which was not controlled was also compared and is the difference between the R^2I_p current moment and $R_0^2I_p$ where R_0 is the unperturbed major radius. A set of coefficients for the linear combination of fields, fluxes, and currents were also derived for this parameter. A least squares straight line fit was removed from both the experimental data and simulation responses to remove their offsets and linear drift. This is because the low frequency disturbance or drift experienced by the plasma was not modelled.

Limited Plasma The closed loop time domain responses of a limited plasma to antisymmetric stimulations were first compared to a rigid current displacement model (RCDM) in [1]. The agreement was found to be good and showed that the coils close to the centre and on the inboard side were best coupled to fast vertical motion of the plasma. The RBS data was reanalysed to produce frequency response estimates which were compared with the RCDM and CREATE-L models (Fig.1). Both models agree with the estimated responses and clearly lie within the estimated confidence bounds. It is also confirmed that coil-pair E4-E5 has a much larger closed loop amplitude response at frequencies above 10Hz than the pair F1-F8 and has a smaller phase lag.

Symmetric excitation first introduced in [2] was used to examine up-down symmetric parameters. The RCDM cannot model these outputs and instead the CREATE-L model and a plasmaless CREATE-L model were compared to the experiment. Since the TCV controller design was based on a plasmaless model the latter was thought to be a useful comparison. The CREATE-L model is within good agreement for all coils and parameters in both the time and frequency domains. The plasmaless model does not provide a meaningful signal in the case of the plasma current moment parameters but is reasonable when compared to the P_VERT, TRI_OUT and TRI_IN signals.

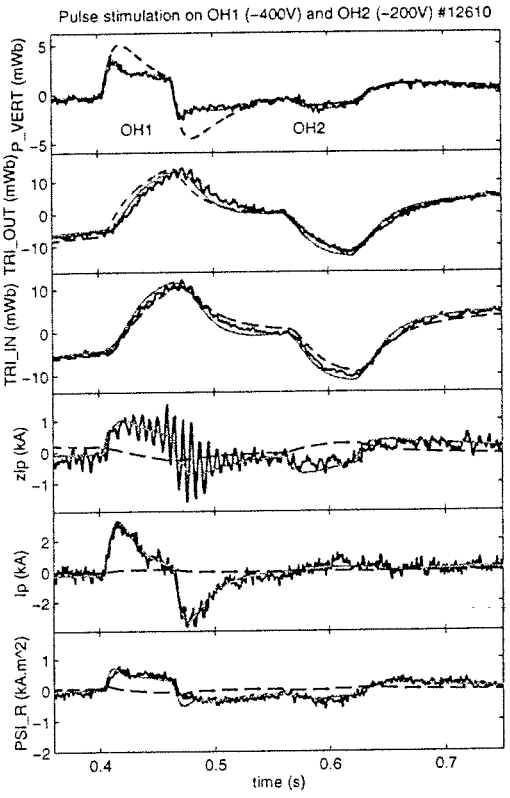

Fig.2 Response of SND plasma to square pulse stimulation for expt. (dark solid), CREATE-L (light solid) and plasmaless model (dashed)

Diverted plasma The analysis was repeated for a single-null diverted plasma with single coil excitation. The CREATE-L model proved to be in good agreement with all the parameters except zI_p (Fig.2). The model follows the experimental trace except for oscillations in the experiment which occur when the plasma radial position moves a significant distance. This can be explained by nonlinear coupling of the zI_p dynamics to the position of the plasma. As the plasma moves radially outwards the vertical gradient of the radial field ($\delta B_R/\delta z$) causes an increase in the plasma vertical position instability growth rate. The closed loop plant becomes highly underdamped and begins to oscillate at the resonant frequency (130Hz).

The response of the separatrix was considered important and was compared. Plasma equilibrium parameters and the plasma contour were reconstructed using the LIUQE inverse equilibrium code [3] from both experimental and simulated measurements of the poloidal field, flux and control coil currents. Parameters such as l_i, β_p and q_a were in agreement (Fig.3) as well as shape parameters such as κ, δ and the plasma contour itself.

Model assumptions Two variants of the CREATE-L model were tested on the diverted configuration in order to examine the effect of the basic assumptions. First the sensitivity of the responses to the shape of the plasma was examined. An up-down asymmetric limited plasma model was created with a similar shape to the diverted plasma. Comparing the simulations to the diverted experiments shows (Fig. 4) that the directly measured parameters are modelled as well as the diverted model except PSI_R. The radial current moment proved to be a sensitive indicator of the model accuracy.

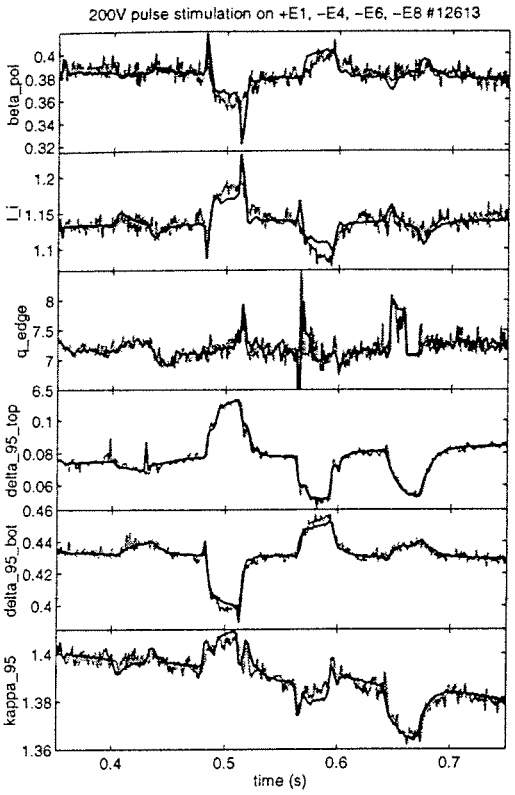

Fig.3 Response of SND plasma to square pulse stimulation for expt. (dark solid) and CREATE-L model (light solid)

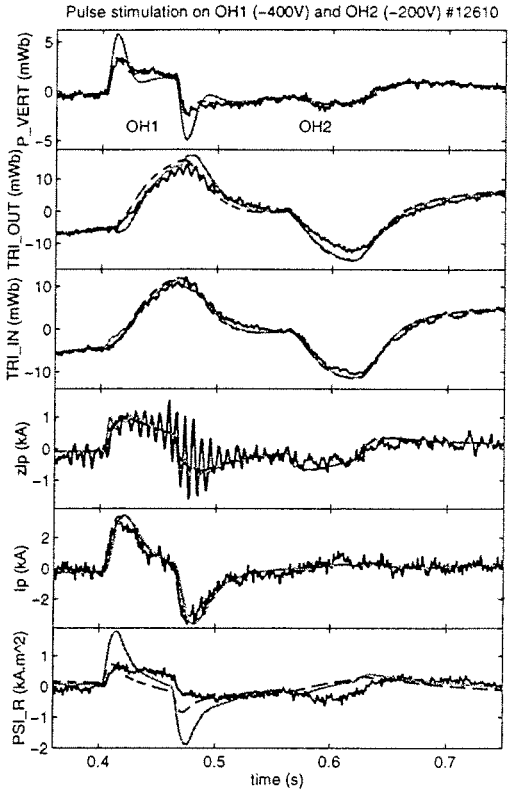

Fig.4 Response of SND plasma to square pulse stimulation for expt. (dark solid), frozen flux CREATE-L (light solid) and limited asymmetric CREATE-L model (dashed)

A second CREATE-L model was created for the diverted plasma assuming that flux at the plasma boundary was frozen. The model agreement with the radial position signals is poor particularly when OH coil stimulation causes large I_p changes to occur. This suggests that this assumption is not reasonable for the closed loop square pulse responses of the plasma.

Conclusions So far no disagreement has been found between any of the closed loop experimental data and the CREATE-L simulations. This suggests that the assumptions made in the derivation of the model are appropriate for plasma position and shape response simulations for the discharges studied.

References

[1] J.B.Lister, Y.Martin and J.-M.Moret, Nuclear Fusion, **36**, 1547 (1996)

[2] F.Villone, P.Vyas, J.B.Lister, R.Albanese, Lausanne Report 569/97 (1997) (submitted to Nuclear Fusion)

[3] F.Hoffman, G.Tonetti, Nuclear Fusion, **28**, 1871 (1988)

This work was partially supported by the fonds national suisse.

MHD stability of configurations with distorted toroidal coils

W. A. Cooper and A. Ardelea
CRPP/EPFL, Association Euratom/Confederation Suisse,
Lausanne, Switzerland

1. Introduction

One of the principal advantages of tokamak/torsatron hybrids is that vacuum flux surfaces exist prior to the current ramp-up and subsequent to the current ramp-down phases. This can facilitate plasma breakdown, reduce volt-second consumption making it possible to lengthen the duration of a discharge and more easily control the termination stages of shots. The added flexibility of an externally applied transform is another favourable consideration, but it is realized at the expense of a nonaxisymmetric deformation of the plasma which can cause the guiding centre drift orbits of particles to escape the confinement zone. Moroz has proposed a compact stellarator/tokamak device [1], but the ideal magnetohydrodynamic (MHD) stability properties of such a concept have not previously been reported. In this paper, we examine the ballooning mode stability and the Mercier criterion of the EPEIUS compact tokamak/torsatron hybrid proposal [2]. We model the EPEIUS coils by single straight filament segments located at their respective centres. The EPEIUS coil set, as shown in Fig. 1, consists of 8 nonplanar toroidally distorted D-shaped coils with $360kA$ current in each. These coils impose an eightfold toroidal periodicity on the system. In addition, there are 3 pairs of vertical field coils. In the absence of a toroidal plasma current in vacuo, the magnetic field lines generate bean-shaped flux surface with varying ellipticity E and triangularity δ depending whether the cross section lies roughly under the plane of a coil (largest E, smallest δ) or between two coils (smallest E, largest δ).

The vacuum magnetic fields are determined using the Biot-Savart law and serve as input for the free boundary version of the three dimensional (3D) VMEC equilibrium code [3]. With vanishing toroidal current, the equilibrium computed reproduces to a very high approximation the last closed flux surface calculated tracing vacuum magnetic field lines. We have studied sequences of equilibria at finite β with zero net toroidal current within each flux surface and with $50kA$ peaked toroidal current. We have also considered a sequence with variable hollow toroidal current fixed at 180 kA and constant $\beta = 6.75\%$. The inverse rotational transform q at the plasma edge is slightly larger than 2 for these values of current and β. The local ideal MHD stability properties of these configurations have been investigated with the relevant modules of the 3D TERPSICHORE code [4].

2. Local ideal MHD stability

The sequence that has zero net toroidal current is obtained with vertical field coil currents $I_v = (120, 180, 180)kA$. The vertical field coil pair that carry $120kA$ have the largest radii at $r_v = 1.06m$. The pairs of concentric coils with centres farthest from the geometric origin each carry $180kA$. The plasma mass profile is prescribed as $M(s) = M(0)(1-s)^3$, where $0 \leq s \leq 1$ is proportional to the toroidal magnetic flux (hence to the plasma volume enclosed). To obtain the corresponding pressure profile, we have chosen the adiabatic index $\Gamma = 5/3$. The q-value increases slightly with β

only near the plasma edge; it decreases slightly for $s \leq 0.6$. The ballooning eigenvalue and the Mercier criterion predict stability up to $\beta \sim 0.8\%$. The edge region $s > 0.6$ tends, however, to remain very spiky. The most unstable ballooning structures localise on the outside edge of the cross section that lies equidistantly between two coils. The sequence with $50kA$ peaked toroidal plasma current has $I_v = (132, 198, 198)kA$ with the plasma mass profile prescribed as $M(s) = M(0)(1-s)^2$ and the toroidal plasma current profile precribed as $2\pi J'(s) = 2\pi J'(0)(1-s)^2$. In this case, the local ideal MHD modes predict basic stability to $\beta \sim 1.2\%$. Locally unstable spikes remain that are closely aligned with resonant values of the inverse rotational transform per field period $1/(qL) = n/m = 1/14, ..., 1/18$, where $L = 8$ is the number of periods. At $\beta \sim 1.4\%$, ballooning modes are unstable for $s > 0.4$. We concentrate in this paper on the $\beta = 6.75\%$, $180kA$ sequence with varying hollow toroidal current profiles. For this sequence, the vertical field coil currents were $I_v = (180, 270, 270)kA$, the plasma mass profile is prescribed as $M(s) = 0.5M(0)[(1-s)^3 + (1-s)^2]$ and the toroidal current profile is prescribed as $2\pi J'(s) = 2\pi J'(0)[c(1-s^5)^2 + (1-c)(1-s^4)^2]$, where the parameter c controls the degree of hollowness of the current profile. We have chosen values of $c = 1, 10, 15, 20, 15$ in this work. The case with $c = 1$ corresponds to a broad monotonically decreasing profile and increasing c enhances the hollow nature of the profile. The toroidal current profiles described this way and the corresponding q profiles are displayed in Fig. 2. The Mercier criterion profiles and the ballooning eigenvalue profiles are shown in Fig. 3. The plasma is unstable for $c \leq 15$. The configuration with $c = 20$ becomes marginally stable to the local stability criteria except at a few isolated and radially very localised surfaces in the outer half of the plasma volume that remain Mercier unstable. The radial location of the point where ballooning stability becomes marginal occurs in the region of vanishing global magnetic shear close to the plasma boundary $s \sim 0.92$. We have verified that the 15 poloidal transit domain of integration for the ballooning calculation on the most unstable field line suffices to resolve the mode structure more than adequately at this radial position.

3. Summary and discussion

In summary, we have investigated the local ideal MHD stability properties of a compact tokamak/torsatron configuration that models the proposed EPEIUS device. The β limits imposed by the Mercier criterion and ballooning modes approach 1% in $50kA$ peaked toroidal current and in current-free cases. A sequence at $\beta = 6.75\%$ is demonstrated to become marginally stable to local modes when the $180kA$ toroidal current prescribed becomes sufficiently hollow that the maximum value of the inverse rotational transform q_{max} exceeds 5 and the minimum value q_{min} near the plasma edge approaches 2. The stabilisation mechanism is associated with the shape of the flux surface average of the parallel current density $< \sigma >$. A $< \sigma >$ profile that increases in magnitude radially exercises a strong stabilising influence on the energy principle [5]. In the outer half of the plasma volume, the Mercier criterion (and to a lesser extent the ballooning eigenvalue) displays very local unstable spikes that align with rational values of $1/(qL)$. We interpret this as a potential for pressure-driven island formation rather than a strict stability limit. This phenomenon requires more detailed investigation using equilibrium codes that can study magnetic island structures. Global internal and external mode stability properties must also be examined, particularly for hollow current profile cases where the large toroidal plasma current concentrated near the plasma edge could destabilise external modes.

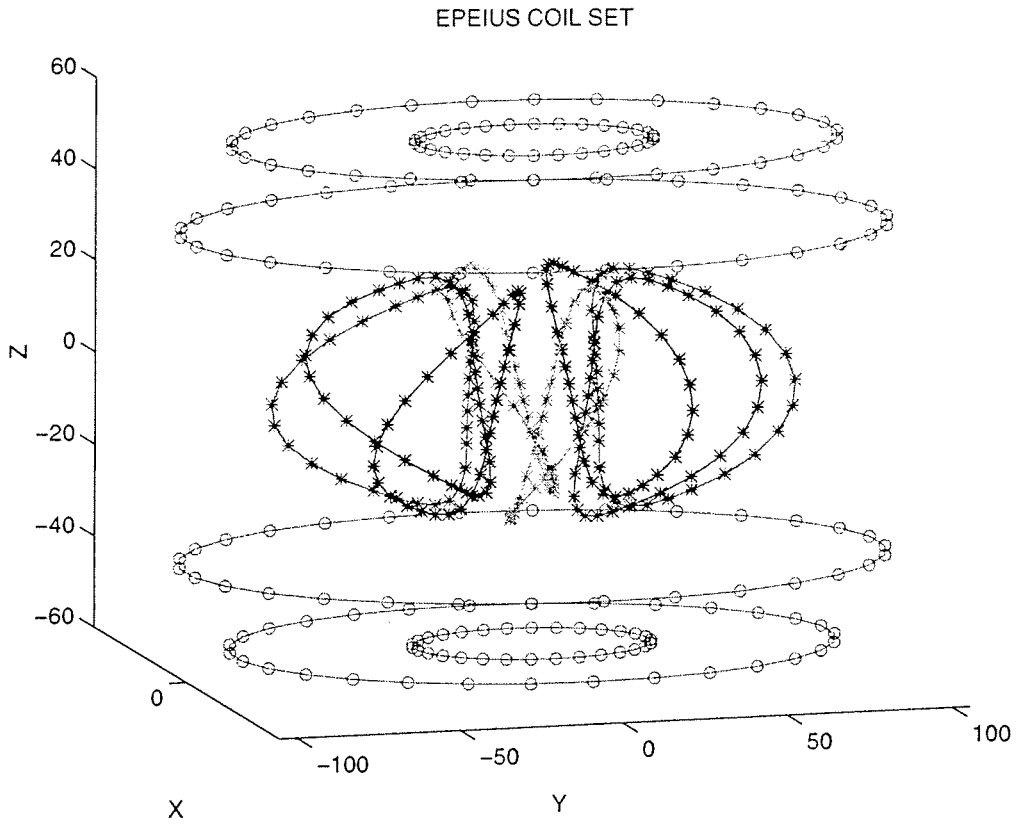

Fig. 1. The EPEIUS coil set consists of 8 identical distorted toroidal coils and 3 pairs of vertical field coils. The coils are modelled by a single filament at their respective centres.

Acknowledgments. We thank P. M. Valanju, J. C. Wiley and A. J. Wootton for providing us a detailed description of the EPEIUS coil system design. We are grateful to S. P. Hirshman for the use of the VMEC code. This research was partially sponsored by the Fonds National Suisse de la Recherche Scientifique and by Euratom.

References

[1] P. E. Moroz, *Phys. Rev. Lett.* **77** 651 (1996)
[2] D. W. Ross et al., *Proc. US/Japan JIFT Workshop, Columbia Univ.* (1996)
[3] S. P. Hirshman et al., *Comput. Phys. Commun.* **43** 143 (1986)
[4] D. V. Anderson et al., *Int. J. Supercomp. Appl.* 4 34 (1990)
[5] W. A. Cooper, *Nucl. Fusion* **34** 729 (1994)

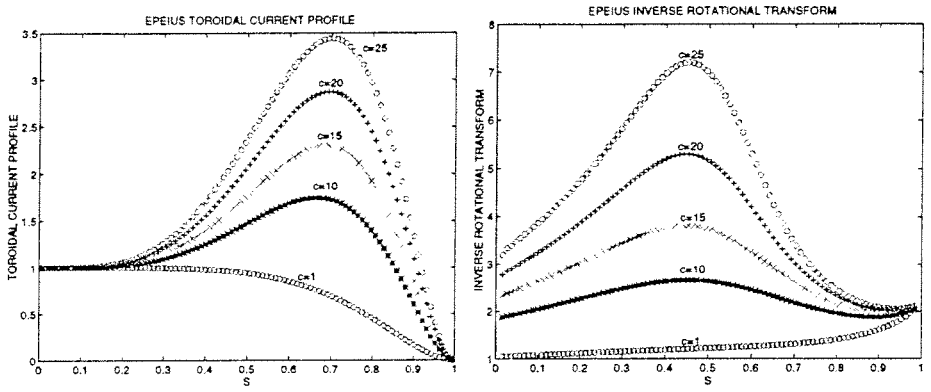

Fig. 2. The toroidal current profiles $2\pi J'(s)$ (left) and the corresponding inverse rotational transform profiles $q(s)$ (right) in an EPEIUS configuration at $\beta = 6.75\%$ with varying degrees of hollowness controlled by the parameter $c = 1(o), 10(*), 15(\times), 20(+)$ and $25(o)$. The toroidal current is $180kA$.

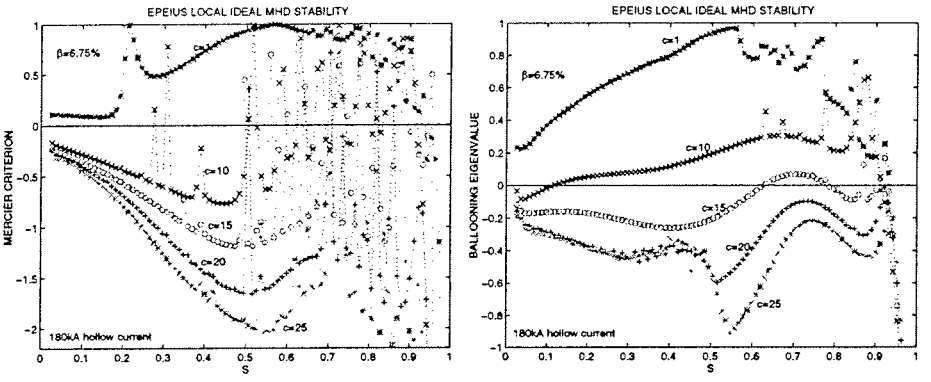

Fig. 3. The Mercier criterion (left) and the ballooning eigenvalue (right) profiles in an EPEIUS configuration with $180kA$ hollow toroidal current at fixed $\beta = 6.75\%$ for values of $c = 1(*), 10(\times), 15(o), 20(+)$ and $25(*)$. Positive values denote instability.

Beta Limits Against External Kink Modes in Tokamaks Taking into Account Plasma Outside Separatrix

L. Degtyarev, A. Martynov, S. Medvedev
Keldysh Institute of Applied Mathematics
Russian Academy of Sciences, Moscow
L. Villard
Centre de Recherches en Physique des Plasmas
Association Euratom - Confédération Suisse
Ecole Polytechnique Fédérale de Lausanne

1 Introduction Pressure driven external kink modes are believed to set an upper limit for the values of β in tokamaks [1]. Extensive investigations of the β limit dependence on plasma geometry and profiles were performed for single axis plasmas. However self consistent modeling of divertor plasma configurations with separatrix at the boundary requires taking into account plasma outside the separatrix. This is evident in the case of typical H-mode profiles with current density and pressure gradients non vanishing at the separatrix. The same question holds for doublet configurations. The codes CAXE and KINX were developed [2] to compute equilibrium and stability of the axisymmetric plasma configurations with separatrix.

The first question to answer is related to a simple case of pressureless and currentless mantle plasma outside the separatrix. Such a case can be readily treated with conventional equilibrium and stability codes for single axis plasma: the equilibrium outside the separatrix was just the same as vacuum. However the current perturbations in a conducting mantle plasma can make the stability of such a configuration different from the traditional approach with vacuum instead of mantle. The difference does take place for axisymmetric $n = 0$ stability. The surface current perturbations play stabilizing role for vertical plasma instability in the case of up-down non symmetric plasma cross section [3]. The mantle plasma outside the separatrix does not considerably change external kink β limits in doublets [4].

For the equilibria with a current density pedestal at the plasma boundary the self consistent modeling of separatrix plasma demonstrates more specific features even still in the frame of ideal MHD approach. Finite current density at the plasma edge brings a question of peeling mode stability. As the peeling mode stability is extremely sensitive to the proximity of vacuum rational magnetic surface to the plasma boundary, the questions arise: what is the plasma boundary and whether it is satisfactory to stay with its conventional ψ_{95} definition. Including the plasma outside the separatrix into the model gives more consistent answer to these questions [5].

Finite pressure gradient in plasma outside the separatrix affects not only localized peeling modes but also global external kink mode stability limits.

2 External kink mode limits in doublets External kink modes in doublet configurations are not restricted to the inside of the separatrix: the perturbations in the outside plasma are as high as inside (Fig.1). Therefore the overall β limit depends on the pressure gradient in the plasma outside separatrix too. Several examples of doublet equilibria with different current density values at the separatrix, different outside plasma layer thickness and several types of pressure gradient profiles outside the separatrix are considered below.

Doublet equilibria with the up-down symmetric boundary (aspect ratio $A = 3.8$, elongation $\kappa = 3.2$) [3] fitted into the TCV vacuum chamber were used in the computations.

The "H-mode" type plasma profiles, with pressure gradient having a maximum at the separatrix and finite separatrix current density, were prescribed by

$$\begin{aligned} I^* &= 1-(1-I_s)\bar{\psi}^{in}, \quad p' = p_s\bar{\psi}^{in}, \quad \text{inside separatrix} \\ I^* &= I_s(1-\bar{\psi}^{out}), \quad p' = p_s(1-\bar{\psi}^{out})^{\alpha_p}, \quad \text{outside separatrix} \end{aligned} \tag{1}$$

where $0 < \bar{\psi}^{in,out} < 1$ are the normalized poloidal fluxes inside and outside the separatrix, respectively, I_s is the value of the current density at the separatrix, p_s is the maximal

value of the pressure gradient at the separatrix: I' is the surface averaged toroidal current density. The plasma profiles of a typical equilibrium are given in Fig.2.

In the first series the current density pedestal value is fixed: $I_s = 0.1$. The limiting values of $g = 2\beta/(I_p/aB) \times 100$ for doublet plasmas are computed against the $n = 1$ external mode stability with a conducting wall sufficiently far from plasma. The factor 2 in the definition the g value is used for easier comparison with the corresponding values in single axis configurations. The value of safety factor at the magnetic axis is $q_0 = 1.05$. Fig.3a presents the results of the stability limit calculations for different values of normalized flux outside separatrix ψ_s (different outside plasma layer thickness): the value of $\psi_s = 1$ corresponds to initial doublet configuration with the ratio of the outside poloidal flux to the total flux inside the plasma 0.19, $\psi_s = 0$ corresponds to a doublet with all plasma outside separatrix removed.

The limiting value g for the single axis plasmas inside the separatrix is $g = 3.65$. The doublet limiting value $g_{\rm lim} \simeq 3.5$ at $\psi_s \to 0$ (when the mantle plasma is very thin) is not far from the single axis plasma value. The limit is getting lower when the plasma outside the separatrix with finite pressure gradient is building up. The decrease in the g value limit is bigger when the exponent α_p is lower in outside pressure gradient profile (1) which corresponds to higher values of pressure at the separatrix.

The difference between the values of $g_{\rm lim}$ at $\psi_s = 0$ and $\psi_s = 1$ is about the same for toroidal wave number $n = 2$: $g_{\rm lim} = 3.84$ and $g_{\rm lim} = 3.14$ respectively ($\alpha_p = 1$).

Localized ballooning mode criterion gives instability at $g \simeq 2.2$ ($\alpha_p = 1$) for the plasma near the separatrix from inside: marginally stable values of p' are shown in Fig.2 with dashed line. The plasma outside the separatrix is stable against localized ballooning modes for all considered equilibria and seems to be in the second stability region.

In the next two series the value of the current density at the separatrix changes ($\alpha_p = 1$). The value of the safety factor at magnetic axis is either fixed $q_0 = 1.05$ (Fig.4a) or adjusted to give total normalized current in doublet $I_N = I_p/(aB) \simeq 1.1$ (Fig.4b). The difference between the single axis and doublet limits in g is about the same versus the value of current density at the separatrix I_s when the normalized current is not too high (Fig.4a for $I_s < 0.2$ and Fig.4b).

Keeping the values of q_0 fixed and raising the value of I_s leads to an increase in the value of normalized current. The values of q_{95} in the plasma inside the separatrix are less than 2 for $I_s > 0.3$ and the current limit corresponds to $I_s = 0.34, I_N = 1.8/2$ for single axis plasma. The current limit in doublets with increasing I_s is higher: $I_s = 0.67, I_N = 2.4$. Still the limiting g values are very low: $g_{\rm lim} < 1$ at $I_s > 0.4$. However the decrease in the limiting g values for single axis as well as doublet plasmas also takes place at relatively low value of normalized current $I_N = 1.1$ (Fig.4b). It is connected with higher values of q_0 and lower global shear.

Pressure gradient profiles with a maximum at the separatrix is close to optimal concerning the external kink mode stability of single axis plasma. The last series of stability computations confirms the above results for another class of pressure gradient profiles still close to the "H-mode" profiles but with $p' = 0$ at the separatrix. They are produced from the initial profiles (1) by multiplication by $(1 - \psi_{in})^{0.5}$ inside the separatrix and by $\psi_{out}^{0.5}$, ψ_{out} and 0 outside the separatrix (Fig.5abc). The value of g limit for single axis plasmas is very close to the result with the initial profile $g = 3.65$. The limiting value for the doublets is quite unexpectedly goes down despite of lower values of pressure gradient: from $g_{\rm lim} = 2.9$ to $g_{\rm lim} = 2.5$ (compare Fig.2 and Fig.5a). At the same time the plasma outside the separatrix is not in the second stability region of ballooning modes. Still lower values of pressure gradient (Fig.5b) give again an increase in doublet limiting value $g_{\rm lim} = 3.15$. Finally the doublet limit is practically the same as for single axis plasma in the case of force free outside plasma $g_{\rm lim} = 3.65$ (Fig.5c).

3 Stability of divertor configurations The divertor equilibria with plasma outside the separatrix can be treated with the divertor versions of the CAXE and KINX codes. A characteristic feature of a divertor configuration is a presence of open magnetic field lines penetrating the end plates. The boundary conditions at the end plates are discussed in [5].

The choice of vanishing displacement condition at the end plates (fixed plates) leads

to a strong stabilizing effect of the plasma outside separatrix. Fig.3b present the results of stability calculations analogous to that of Fig.3a for doublets. The dashed curves show a growth of the limiting g values with a thickness of the plasma outside the separatrix independently of the pressure gradient profile.

Another choice is to use natural boundary conditions at the end plates following from the variational formulation of the stability problem and leave the boundary conditions for vacuum solution the same as in the fixed plates case. The resulting model does not include the stabilizing vacuum potential energy perturbations corresponding to the non zero perturbations at the end plates and omits the additional surface term in the potential energy [5] and therefore is not self-consistent. However the g limits according to that model behave in the same way as the limits in doublets with increasing pressure gradient in the outside plasma (Fig.3b, solid lines). The decrease in $g_{\rm lim}$ with higher pressure at the separatrix is less pronounced in the divertor case than in the case of doublets.

One of possible extensions of the model is the inclusion of positive vacuum energy contribution due to the plasma displacements at the end plates.

4 Conclusions The pressure profile variation in relatively thin plasma layer outside the separatrix can influence global external kink mode stability and considerably change the β limit in doublet configurations.

The conclusions for divertor configurations strongly depend on the choice of boundary conditions at the open field lines. Fixed boundary conditions at the divertor end plates result in stabilizing effect of the plasma outside separatrix independent of pressure gradient there. More realistic choice of boundary conditions gives a behavior similar to the doublet case.

References

[1] Troyon F. *et al.* Plasma Phys. and Contr. Fusion 26 (1984) 209

[2] Degtyarev L., Martynov A., Medvedev S., Troyon F., Villard L., Gruber R. The KINX ideal MHD stability code for axisymmetric plasmas with separatrix. Comput. Phys. Commun. (1997) to appear

[3] Degtyarev L., Martynov A., Medvedev S., Troyon F., Villard L. Influence of plasma near separatrix on ideal MHD stability in tokamaks. 22th EPS Conf. on Controlled Fusion and Plasma Phys., Bournemouth, Proc. Contrib. Papers Vol.19C, Part I (1995) 217

[4] Degtyarev L., Martynov A., Medvedev S., Troyon F., Villard L. MHD limits and axisymmetric stability of doublets. 21th EPS Conf. on Controlled Fusion and Plasma Phys., Montpellier, Proc. Contrib. Papers Vol.18B, Part II (1994) 556

[5] Degtyarev L., Martynov A., Medvedev S., Troyon F., Villard L. External kink mode stability of tokamaks with finite edge current density in plasma outside separatrix. 23th EPS Conf. on Controlled Fusion and Plasma Phys., Kiev, Proc. Contrib. Papers Vol.20C, Part III (1996) 1191

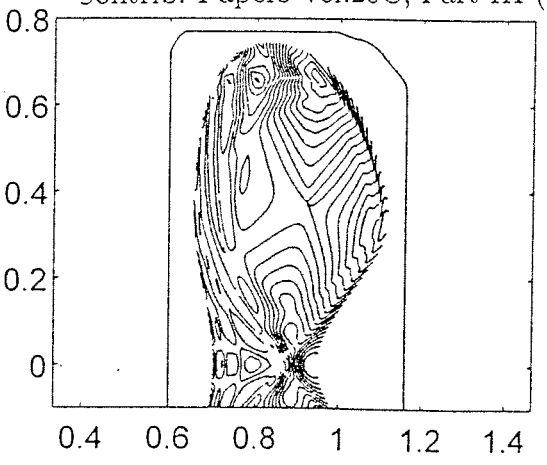

Fig.1. External pressure driven kink mode structure in doublet equilibrium, $g = 4.3$. Normal displacement level lines. $\omega^2/\omega_A^2 = -1.5 \cdot 10^{-3}$

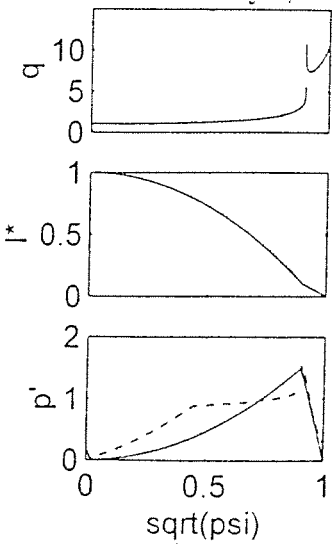

Fig.2. Plasma parameter profiles for doublet equilibrium, $g = 4.3$.

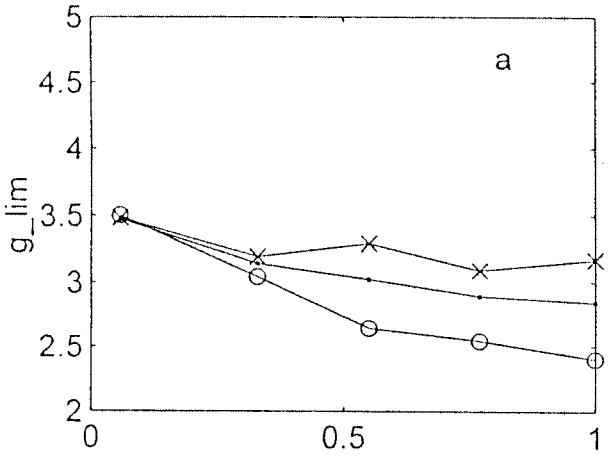

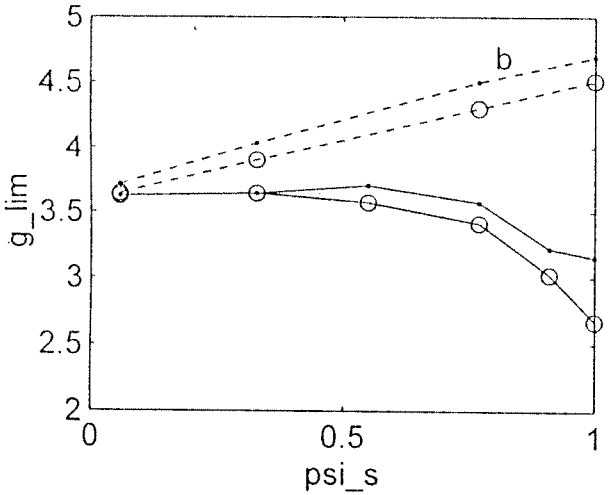

Fig.3. Limiting g values against external $n = 1$ kink mode versus normalized flux in outside plasma, points - $\alpha_p = 1.0$, circles - $\alpha_p = 0.5$, crosses - $\alpha_p = 2.0$. a) doublet b) divertor, solid lines - free plates, dashed lines - fixed plates.

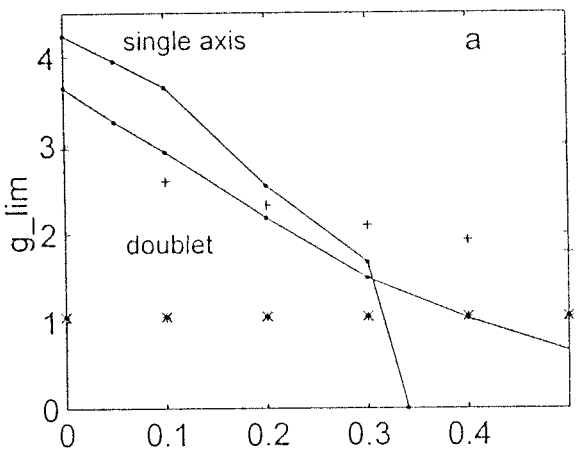

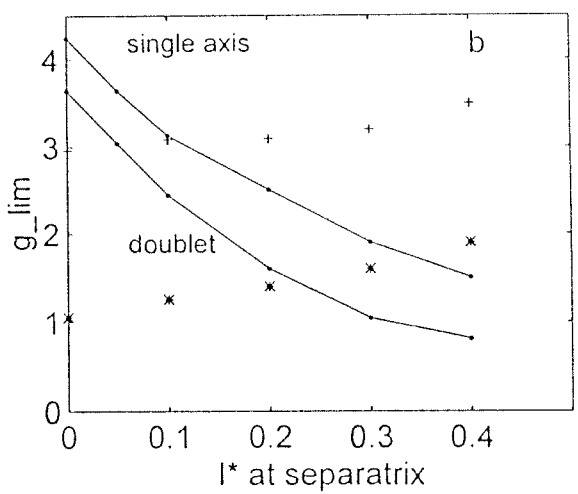

Fig.4. Limiting g values against external $n = 1$ kink mode for doublets versus current density at separatrix, crosses - q_{95} values, stars - q_0 values. a) $q_0 = 1.05$ b) normalized current $I_N = 1.1$

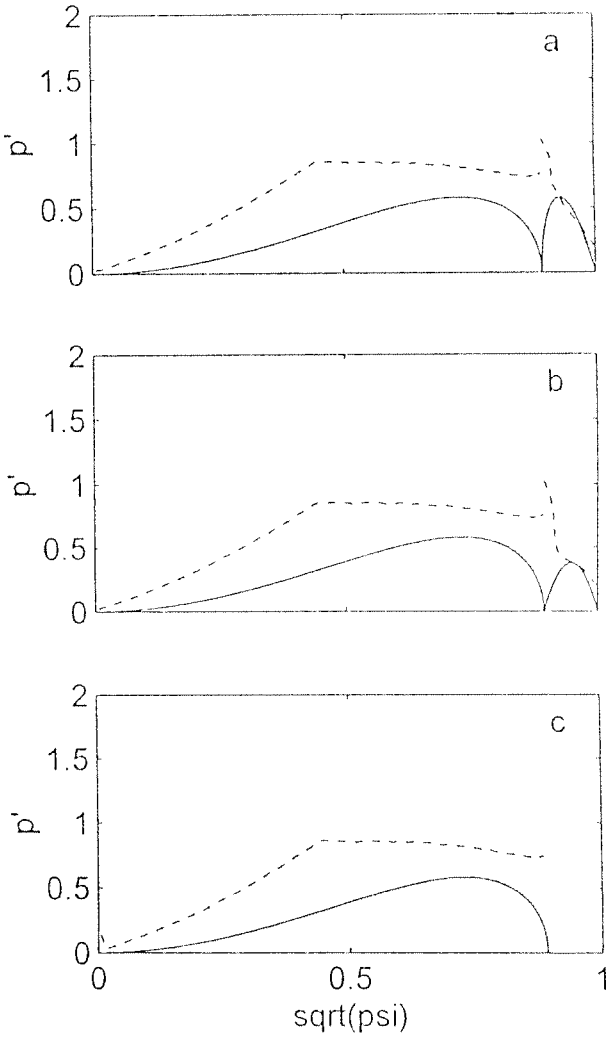

Fig.5. Pressure gradient profiles with $p' = 0$ at separatrix for doublet equilibria

Few Period Quasisymmetric Stellarators

M.Yu. Isaev, W.A. Cooper*, S.Yu. Medvedev+, M.I. Mikhailov,
V.D. Shafranov, **A.A. Subbotin**

Russian Research Centre "Kurchatov Institute", 123182, Moscow, Russia
* Centre de Recherches en Physique des Plasmas, Association Euratom-Confederation Suisse, Ecole Polytechnique Federale de Lausanne
+ Keldysh Institute of Applied Mathematics, Russian Academy of Sciences, Moscow

1. Introduction

The results of plasma equilibrium and local stability investigations in two and four-period quasisymmetric stellarators are presented. A near-axis approximation is used for 2-period systems and the 3D codes VMEC and TERPSICHORE are used for four-periods devices to optimise the configurations.

2. Four-period Heliac-like configurations

In this Section, the results of the partial optimisation of four-period Heliac-like magnetic configurations by plasma boundary control are presented. We use the term "Heliac-like" configuration for systems in which the magnetic surface cross-section rotates in phase with the principal normal with respect to the magnetic axis, $n_1 = 0$. Here n_1 constitutes the number of elliptical near-axis magnetic surfaces cross-sections turns relative the principal normal to the magnetic axis in one field period. Helias-like configuration such as the well-known WVII-X have $n_1 = -1/2$.

We look for the shape of the plasma boundary for which the Mercier $< \beta >$ limit is maximal and the accuracy of fulfilling the quasisymmetry (QS) condition is moderate, $X \approx 3$. Here X is the ratio of dominant helical Fourier component of the magnetic field strength in Boozer coordinates to the maximal Fourier component that violates the symmetry evaluated at the plasma boundary.

The plasma boundary surface obtained from the QS condition in the near-axis approximation, Ref. [1], was used here as the initial guess. After optimisation of the plasma boundary with the VMEC and TERPSICHORE codes to increase the $< \beta >$ limit with respect to Mercier mode stability, we have found the configuration with the following boundary Fourier spectrum:

MB	NB	RBC	ZBS
0	0	9.9520E-00	0.0000E+00
0	1	2.3600E-00	-2.1200E-00
0	2	1.5000E-01	-1.5000E-01
1	0	6.5000E-01	7.3000E-01
1	1	-7.0000E-02	7.0000E-02
1	2	-2.9300E-01	2.6500E-01
1	3	6.1000E-02	-6.1000E-02
1	4	1.0000E-02	-1.0000E-02
2	0	-6.0000E-02	-6.0000E-02
2	1	7.0000E-02	7.0000E-02
2	2	-1.2500E-01	-1.5000E-02
2	3	7.1000E-02	-7.1000E-02
2	4	-1.0000E-03	1.0000E-03

The equilibrium $< \beta >_{eq}$ limit in this configuration equals 9.8%. Magnetic surface cross-sections are shown on Fig. 1. For $< \beta >= 3.5\%$, the Fourier spectrum of the magnetic field strength in Boozer coordinates is shown in Fig. 2. The dependencies of the Mercier criterion and the ballooning eigenvalues on the radial variable s that labels the magnetic surfaces (s is proportional to plasma volume enclosed) are shown in Fig. 3. It is seen that the $< \beta >_M$ limit is about 4% and the ballooning $< \beta >$ limit is $< \beta >_B = 1.4\%$. The plasma pressure was considered as parabolic ($p'(s)$ is const).

One can see that there exists a rather large difference between $< \beta >_M$ and $< \beta >_B$. Since this configuration was found by optimization of the Mercier criterion, it is worth to try to modify the plasma boundary to get larger a $< \beta >_B$. Retaining the accuracy of the QS condition fulfillment to X=3, the result of such an attempt was the sharp diminishing of the $< \beta >_M$ with only a modest increase of $< \beta >_B \approx 1.6\%$.

In the Heliac-like systems considered as well as in Helias-like QS stellarators, Ref. [2,3], the very localised ballooning modes along the magnetic field lines are the most dangerous. The optimisation carried out here cannot be considered as exhaustive. We have not changed the plasma pressure profile and did not use higher harmonics in the boundary representation (see Table). As mentioned in Ref. [4], these harmonics can be used to improve the quasisymmetry. The availability of a large number of free parameters makes it reasonable to further continue the optimization procedure.

3. Two-period quasisymmetric configurations

Recently the most compact two-period quasisymmetrical stellarator systems of the figure-eight type were found numerically. They became the basis for a project MHH-2, Ref. [5] under development in the USA, and a corresponding project under development in Japan, Ref. [4]. In these systems, the principal normal with respect to the magnetic axis does not rotate relative the "torus hole" (quasiaxial symmetry), while the magnetic surfaces make one-half turn per period.

In this Section, a search of two-period quasisymmetric systems in a wide range of the configuration parameters is undertaken. Calculations were made in the paraxial approximation with the application of a semianalytic method previously developed, Ref. [6]. We have estimated the equilibrium $< \beta >$ limit and the possibility of stabilising the Mercier modes. The elongation and triangularity of the magnetic surfaces at the beginning of a period, the aspect ratio and the ellipticity of the reference torus on which the trajectory of the magnetic axis lies have been optimised. In Fig. 4, the dependencies of the equilibrium $< \beta >$ limit on the toroidicity r_1/R_0 of the magnetic axis reference torus are shown. As is seen, three types of two-period quasisymmetric stellarators exist. They are characterised by the number of magnetic surface cross-section turns in one system period, n_1, with respect to the magnetic axis principal normal.

For small values of r_1/R (cases A and A_1), the principal normal of the magnetic axis does not rotate. Thus, quasiaxial symmetry (QAS) is realized here. The case A corresponds to $n_1 = 1/2$. The magnetic surface cross-sections make one-half turn of rotation per system period with respect to the magnetic axis principal normal. This situation corresponds to those proposed in Ref. [3-5]. In this case we have not found Mercier stable systems. The case A_1 corresponds to $n_1 = 0$. The magnetic surface cross-sections here do not rotate (they only oscillate) with respect to the torus hole. This is a tokamak-like situation with small rotational transform which is Mercier unstable.

When the aspect ratio of the reference torus on which the magnetic axis lies decreases, case B, the principal normal of the magnetic axis rotates, thus quasihelical symmetry (QHS) is realized. When the QS conditions are satisfied, the magnetic surface cross-section rotates in phase with the principal normal, $n_1 = 0$. These systems are Mercier stable up to $< \beta >= 4.5\%$ at $r_1/R \approx 0.45$.

It is worth to emphasize that here we have used the *precise* conditions of QS in the approximation to second order. In this approximation, the shear of the rotational transform is considered to be zero and the precise conditions allow to satisfy the Mercier criterion only for configurations with $n_1 = 0$, whereas the numerical 3D calculations have shown that stabilisation of local modes in two-period QAS configurations with $n_1 \neq 0$ is also possible at the expense of some violation of QS conditions, Ref. [3].

4. Conclusions

The four-period Heliac-like QS configurations studied earlier in the near-axis approximation have been considered here with 3D codes. It is shown that with moderate accuracy of QS, the configurations of such type have $< \beta >$ limits comparable to the widely investigated Helias-like QS configurations.

The possibility of the existence of two-period QS configurations have been studied also. Only the near-axis approximation was used. It is shown that Mercier stable Heliac-like configurations of the figure-eight type do exist. As reported in Sec. 2 of the present paper, the ballooning mode stability condition can decrease the $< \beta >$ limit significantly. 3D Ballooning stability results for two-period $n_1 = 0$ configurations are being examined.

To find stellarator systems with better properties, including higher β and moderate transport, weakening slightly the QS condition could be reasonable, Ref. [7,8].

Acknowledgements

We thank Prof. F. Troyon for supporting this work and Dr. S. P. Hirshman for making the VMEC code available to us. This work was partially supported by the Russian Foundation of Fundamental Research, grant N 97-02-17695, the Fonds National Suisse pour la Recherche Scientifique and Euratom.

References

[1] Isaev M.Yu., Mikhailov M.I., Shafranov V.D., Subbotin A.A.// Proc. of 10th Int. Conf. on Stellarators, **27**, 186(1995). Madrid, 1995, p.278.

[2] Matthews P.G., et al.// in Proc., 10th Int. Conf. on Stellarators, (Int. Atomic Energy Agency Technical Committee Meeting), Madrid, 1995 (IEAE, Vienna, 1995). p.167.

[3] Reiman A.H., Ku L.P., Monticello D.A., Nührenberg C., Cooper W.A. // Plasma Physics Reports **23**, 472 (1997).

[4] Nakajima N., Yokoyama M., Okamoto M., Nührenberg J.// Plasma Phys. Reports **23**, (1997) to be published.

[5] Garabedian P.// Phys. Plasmas 3(7), 1996, 2483.

[6] Isaev M.Yu., Mikhailov M.I.// Plasma Phys. Reports **22**, 43 (1996).

[7] Gori S., Lotz W., Nührenberg J.// Theory of Fusion Plasmas, SIF, Bologna, 1996, Ed. by J.W. Connor, E. Sindoni and J. Vaclavik, p. 335.

[8] Mikhailov M.I., Shafranov V.D., Subbotin A.A., Sunder D.// This conference.

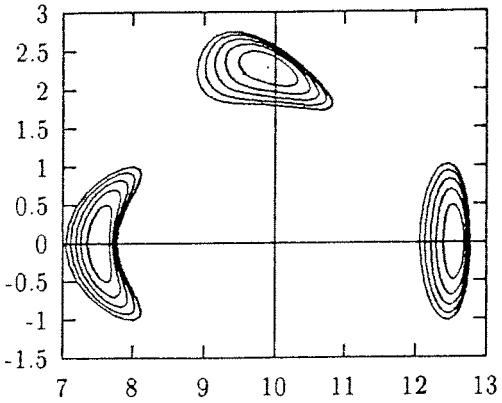

Fig. 1. Magnetic surfaces cross-sections for $< \beta >= 3.5\%$.

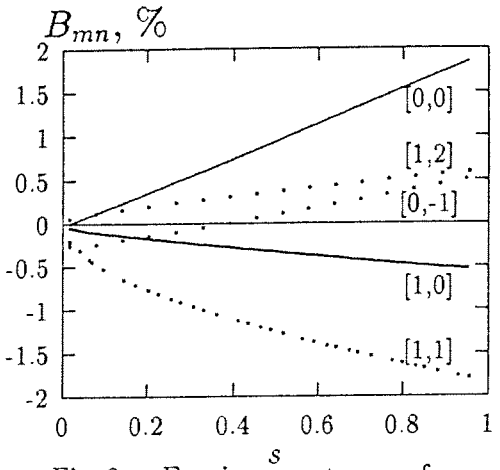

Fig. 2. Fourier spectrum of magnetic field strength in Boozer coordinates for $< \beta >= 3.5\%$ in dependence on radial coordinate.

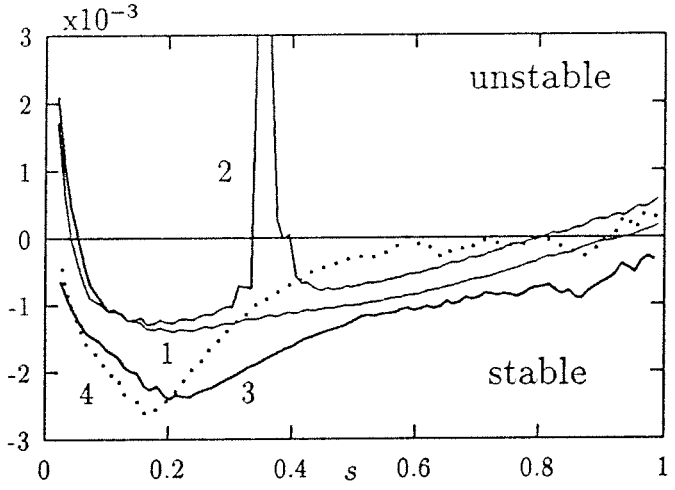

Fig. 3. The dependencies of Mercier criterion and ballooning eigenvalues on s, labeling the magnetic surfaces (s is proportional to plasma volume enclosed).

1 - Mercier criterion for $< \beta >= 3.73\%$
2 - Mercier criterion for $< \beta >= 4.06\%$
3 - Ballooning eigenvalues for $< \beta >= 1.07\%$
4 - Ballooning eigenvalues for $< \beta >= 1.4\%$

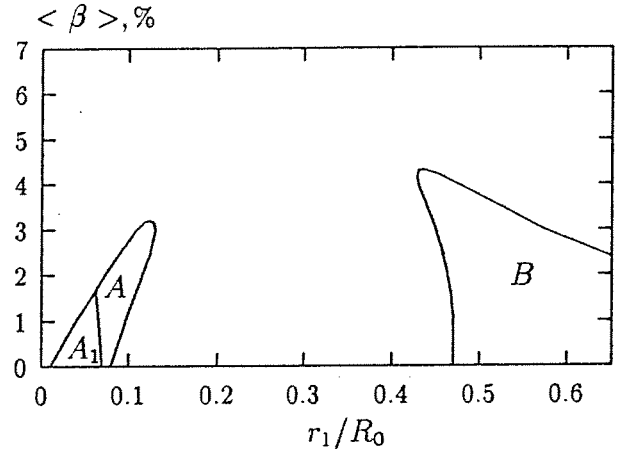

Fig. 4. The dependencies of equilibrium $< \beta >$ limit on the thickness of magnetic axis reference torus. All other parameters are optimal.

A : $n_1 = 1/2$; A_1 : $n_1 = 0$;
B : $n_1 = 0$.

Measurement of the Effective Plasma Ion Mass in Large Tokamaks

J.B. Lister, L. Villard and G. de Ridder
Centre de Recherches en Physique des Plasmas
Association Confédération Suisse-EURATOM, CRPP-EPFL, CH - 1015 Lausanne

ABSTRACT There is not yet a straightforward method for the measurement of the D-T ratio in the centre of a tokamak plasma. One of the simpler measurements put forward in the past is the interpretation of the MHD spectrum in the frequency range of the Global Alfvén Eigenmodes (GAE). However, the frequencies of these modes do not only depend on the plasma mass, but are also quite strongly dependent on the details of the current and density profiles, creating a problem of deconvolution of the estimate of the plasma mass from an implicit relationship between several measureable plasma parameters and the detected eigenmode frequencies. This method has been revisited to assess its likely precision for the JET tokamak. The low *n* GAE modes are sometimes too close to the continuum edge to be detectable and the interpretation of the GAE spectrum is rendered less direct than had been hoped. We present a statistical study on the precision with which the D-T ratio could be estimated from the GAE spectrum on JET.

1. Introduction The ratio of deuterium to tritium ions (D-T ratio) should be close to unity in the plasma core to maximise the thermal fusion power. Different sources of deuterium and tritium from neutral beam injection, pellet injection, gas fuelling and recycling from walls and the divertor make the D-T source ratio difficult to estimate. Different radial transport time constants might further confuse the control of the D-T ratio. For these reasons a direct measurement of the D-T ratio is highly desirable. In the absence of a clear candidate for this measurement, we have revisited the use of Global Eigenmodes of the Alfvén Wave (GAE) for determining the core D-T ratio in the JET tokamak.

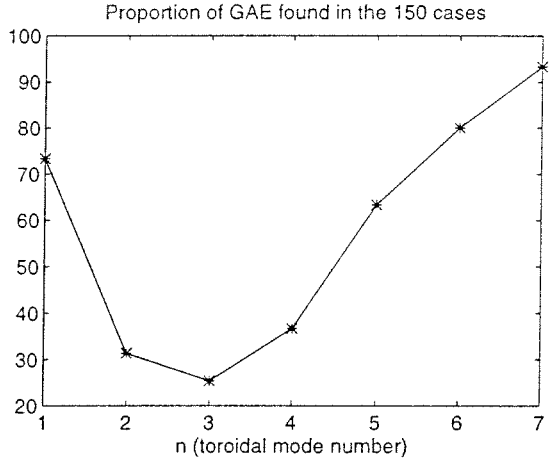

Fig. 1 Percentage of GAEs found in 150 test runs, as a function of the toroidal mode number.

A method of estimating the effective mass, defined as $A_{eff} = \Sigma A_i n_i / n_e$ summing over all ion species, was developed on the TCA tokamak [1,2,3]. The method relies on the dispersion relation for Shear Alfvén Waves, given in the cylindrical approximation and up to second order in ω/ω_{ci} by:

$$\omega_{nm}^2(r) = \omega^{o}_{nm}{}^2(r)/A_{eff}(r)[1+\{\omega^{o}_{nm}{}^2(r)/\omega_{cH}^2\}\{\Sigma n_i(r)A_i^3/n_e(r)Z_i^2\}/A_{eff}(r)^2],$$

where $\omega^{o}_{nm}{}^2(r) = B_\phi^2(n+m/q(r))^2/\mu_0 n_e(r) m_p R^2$, n and m are the toroidal and poloidal mode numbers, ω_{cH} is the cyclotron frequency of hydrogen and the summation is over all ion species. The GAE frequencies lie close to but below the minimum of this continuum frequency. Many GAE's can be detected using a wide-band frequency sweep and A_{eff} could be estimated from the full spectrum of observed GAE's. On TCA, about 60 W were launched by a small poloidal emitting antenna and the system was used to measure the dynamic behaviour of the effective mass following the influx of cold H^0 into a D^+ discharge [2] and to feedback control the H-D ratio [3]. These encouraging results leave us with two open

questions. Firstly, we needed to assess the likely precision for JET and secondly we needed to assess whether the physics of the GAE would be different on a much larger device.

2. Method The uncertainties in using the GAE frequency as a diagnostic lie in its known sensitivity to the precise details of both the plasma current and density profiles which have considerable experimental uncertainty. Although the value of the Shear Alfvén Wave continuum frequency on axis, $\omega_{nm}(0)$, is a local quantity, the separation between $\omega_{nm}(0)$ and the eigenmode frequency ω_{GAE} is not and we must infer the value of this separation from the experimental data available. In order to assess the extent to which the usually measured quantities allow us to estimate this separation, we embarked on a Monte-Carlo based approach to this proposed diagnostic, which required several steps:

- determination of a suitable plasma profile parametrisation
- determination of the realistic parameter ranges
- determination of inter-parameter correlations providing additional constraints
- generation of a large volume of Monte-Carlo plasma parameters
- adjustment of the multi-dimensional population to simulate a realistic distribution
- generation of a small subset of data, creating 150 plasmas to be analyzed.

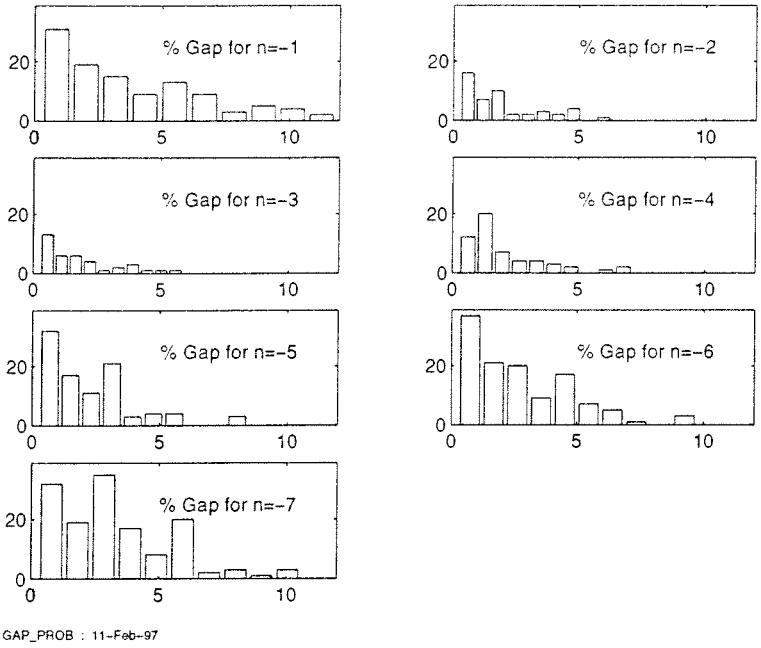

Fig. 2 Histogram of the variation of $\delta\omega/\omega$ for different toroidal mode numbers.

The resulting "representative" JET discharges were then simulated in the 1-D ISMENE code [4] to calculate the GAE frequency for modes $n = -1 \ldots -7$ and $m = -1$. In ISMENE we consider a cold, magnetized, current carrying, bounded plasma, including several ion species and various mass and current density profiles. All 150 plasmas were analysed in this way giving 1050 eigenfrequencies. Full details of the results are to be found in [5].

3. Results A first inspection of the raw results was disappointing due to the large number of gaps in the results where the code had failed to locate a GAE peak in the plasma response, either because the GAE does not exist, or its eigenfrequency is too close to the continuum edge. Figure 1 shows the proportion of the 150 runs producing a separated GAE resonance, as a function of n. The values of $\delta\omega/\omega$ found are histogrammed for different n in Fig. 2, showing a significant variation.

Figure 3 shows the percentage GAE separation as a function of n, for three representative cases. Figure 4 shows the results from a frequency scan across the modes $n = -1 \ldots -7$, $m = -1$ for one case. The vertical bar indicates the continuum edge, ω_{min} = minimum of $\omega_{nm}(r)$, since the continuum may be at the edge of the plasma or at a local off-axis minimum. The frequency scans are shown over the range (0.86 - 1.01) x ω_{min}. The widths and heights of the GAE peaks are defined by an artificial damping term introduced into the cold plasma model. In the case shown, the GAE disappears into the continuum for $n = -2, -3, -4$ but subsequently

reappears. Runs of ISMENE using a 1-D hot model expanded to second order in ion Larmor radius showed the same disappearance into and reappearance from the continuum.

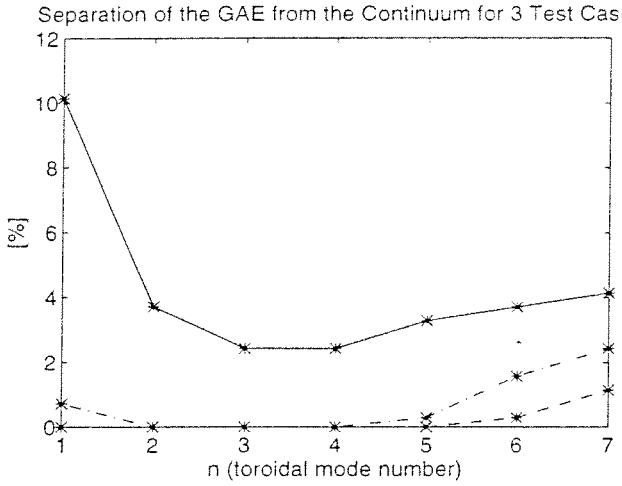

GAE_GAP : 10-Feb-97

Fig. 3 GAE separation $\delta\omega/\omega$[%] as a function of toroidal mode number for the 3 test cases. The solid line is case No 1, the dashed line is case No 14 and the dot-dashed line is case No 12.

We have cross-checked a few cases to confirm the cylindrical model, by performing computations with the finite element LION code [6,7]. LION differs from ISMENE not only by its finite aspect ratio, but also in the fact that no assumption is made on the ratio B_O pol/B_O tor, whereas ISMENE relies on a first-order expansion in B_O pol/B_O tor. The proper modelling of B_O pol/B_O tor in LION has even more dramatic effects, in particular for the lowest frequency modes and low n modes. Indeed, the first order approximation in B_O pol/B_O tor is not valid for $\omega/\omega_{ci} \approx 0$ or for $n = 0$. In simple analytical cases (e.g. $n = 0$, $q = \text{const}$, $\omega/\omega_{ci} \approx 0$) the first order model predicts the existence of GAEs whereas the exact model predicts no GAE. The relatively high fraction (50%) of $n = -1$ cases with GAEs as predicted by ISMENE might therefore be exagerated by an artifact of the first order expansion in B_O pol/B_O tor.

Finite aspect ratio effects have also been checked. The eigenfrequency of the GAE is more affected by toroidicity for low n than for high n. But even for $n = -1$ we found the GAE eigenfrequency changed by less than 3%. Finite aspect ratio also leads to continuum damping of the GAEs through toroidal coupling of shear Alfvén resonance surfaces with different poloidal mode numbers.

To summarise, we have found a smaller fraction of identifiable GAE resonances than initially hoped on the basis of TCA experimental results. The underlying reason is that TCA operated with significant values of the GAE frequency compared with the ion cyclotron frequency ω_{nm}/ω_{ci} ~20-30%. On the other hand the physical size of JET implies ω_{nm}/ω_{ci} of the order of a few percent. Since the ω/ω_{ci} terms push the GAE below the continuum, adding to the separation due to field line curvature effects, the separation between the GAE and the continuum in JET is significantly reduced. ITER would have an even smaller value of ω_{nm}/ω_{ci}. Moreover, the smaller aspect ratio and larger elongation of JET, compared with TCA, increases the toroidal and elliptical coupling of the GAE to Alfvén resonant surfaces of different poloidal mode numbers, thereby increasing the continuum damping of GAEs [6,7]. The response is broadened and flattened and therefore detection of GAEs in JET is almost certainly more difficult than in TCA. The ISMENE results are confirmed as reasonable, provided the probably spurious reappearance of low n modes is ignored.

4. Analysis As a first interpretative step, we fit an MLP (Multi-Layer Perceptron) to the mapping {plasma parameters : $\delta\omega/\omega$}, where the plasma parameters are: [k-j, b-j, k-n, b-n, q*], q* being the cylindrical equivalent (Ip R/a^2 B) and k-j, k-n, b-j, b-n define the radial profiles via the parabolic exponents and edge pedestals respectively. The MLP provides a

generalised functional fitting of an {input:output} multi-dimensional mapping [8]. The values of $\delta\omega/\omega$ for $n = -6$ and $n = -7$ show a high correlation. This implies that little additional information can be obtained by using two adjacent eigenmodes and the analysis was performed just for $n = -7$. The root mean square residual for the full data is ~ 14.8% of its maximum range of 11%, i.e. a statistical precision in ω of 1.6%.The root mean square residual of the actual values of $\delta\omega/\omega$ is 21% of the full range, namely 2.4%. The non-linear MLP prediction of $\delta\omega/\omega$ has therefore only reduced its uncertainty by a factor of 1.5.

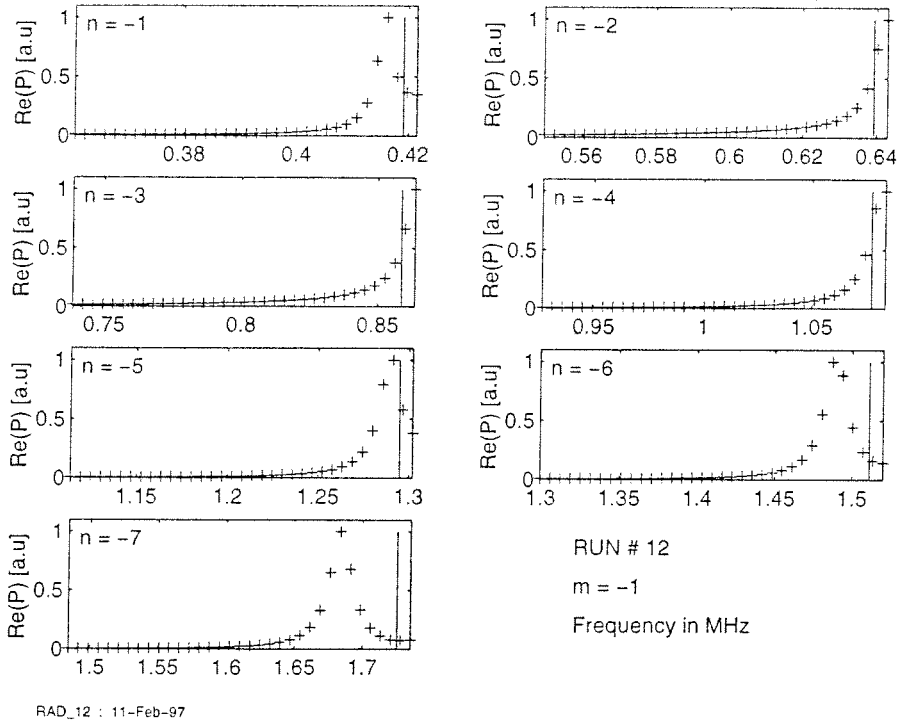

Fig. 4 Spectral scan over the test case # 12.

A simple linear estimation of A_{eff} is obtained if we assume that $n_e(0)$ is experimentally available and we assume $q^o = 1.0$. The resulting value, A_{eff}^o can be fitted by linear regression to the known $A_{eff}(0)$. This relationship between $A_{eff}(0)$ and the estimated A_{eff}^o has an RMS residual of $\sigma = 0.087$. Since the range of $A_{eff}(0)$ is about unity, this corresponds to an RMS residual of 8.7%. An MLP was fitted to the input variables li, k_n, q_{95}, A_{eff}^o to see to what extent an MLP could reduce the uncertainties further. Over the whole dataset for $n = -7$ the full-scale residual was reduced from 5.6% to 5.1% by varying the number of MLP hidden nodes from 1 to 4, illustrating the lack of improvement.

We conclude that the MLP fit to the input data only reduces the uncertainty by a factor of 1.3. We estimate the uncertainty of $A_{eff}(0)$ as being of the order of 7% for the GAE mode $n = -7$, $m = -1$, chosen since it was observed for 140 out of 150 test runs.

ACKNOWLEDGEMENTS The authors would like to thank the JET staff for their interest and contributions, especially J. How as contract coordinator and D.J. Campbell, B. Schunke and A. Tanga. The work was partly supported by JET Article 14 Contract No 950104 and partly by the Fonds national suisse de la recherche scientifique.

REFERENCES

[1] G.A. Collins, A.A. Howling, J.B. Lister, Ph. Marmillod, Plasma Phys. and Contr. Fusion **29**, 323 (1987)
[2] T. Dudok de Wit, B.P. Duval, B. Joye, J.B. Lister, Nuclear Fusion **32**, 359 (1991)
[3] T. Dudok de Wit, J.B. Lister, B.P. Duval, B. Joye, Ph. Marmillod, Nucl. Fusion **30**, 1493 (1990)
[4] K. Appert and J. Vaclavik, in Plasma Physics **24**, 551, (1983)
[5] J.B. Lister, L. Villard, G. de Ridder "GAE detection for mass measurement for D-T ratio control", LRP 574/97 (1997)
[6] L. Villard, K. Appert, R. Gruber, and J. Vaclavik, Comput. Phys. Rep. **4**, 95 (1986)
[7] L. Villard, S. Brunner, J. Vaclavik, Nuclear Fusion **35** (1995) 1173
[8] J.B. Lister, H. Schnurrenberger, Ph. Marmillod, LRP 398/90 (1990)